Antibacterial drug leads targeting isoprenoid biosynthesis

Wei Zhu[a,1], Yonghui Zhang[b,1,2], William Sinko[c,d,1], Mary E. Hensler[e], Joshua Olson[e], Katie J. Molohon[f], Steffen Lindert[c], Rong Cao[a], Kai Li[b], Ke Wang[b], Yang Wang[b], Yi-Liang Liu[a], Anna Sankovsky[b], César Augusto F. de Oliveira[c,g], Douglas A. Mitchell[b,f,h], Victor Nizet[e], J. Andrew McCammon[c,d,g,i,2], and Eric Oldfield[a,b,2]

[a]Center for Biophysics and Computational Biology and [b]Department of Chemistry, University of Illinois, Urbana, IL 61801; [c]Department of Pharmacology, [d]Biomedical Sciences Program, and [e]Department of Pediatrics and Skaggs School of Pharmacy and Pharmaceutical Sciences, University of California at San Diego, La Jolla, CA 92093; [f]Department of Microbiology, University of Illinois, Urbana, IL 61801; [g]Department of Chemistry and Biochemistry, University of California at San Diego, La Jolla, CA 92093; [h]Institute for Genomic Biology, University of Illinois, Urbana, IL 61801; and [i]Howard Hughes Medical Institute, University of California at San Diego, La Jolla, CA 92093

Contributed by J. Andrew McCammon, November 16, 2012 (sent for review October 2, 2012)

With the rise in resistance to antibiotics such as methicillin, there is a need for new drugs. We report here the discovery and X-ray crystallographic structures of 10 chemically diverse compounds (benzoic, diketo, and phosphonic acids, as well as a bisamidine and a bisamine) that inhibit bacterial undecaprenyl diphosphate synthase, an essential enzyme involved in cell wall biosynthesis. The inhibitors bind to one or more of the four undecaprenyl diphosphate synthase inhibitor binding sites identified previously, with the most active leads binding to site 4, outside the catalytic center. The most potent leads are active against *Staphylococcus aureus* [minimal inhibitory concentration ($MIC)_{90}$ ~0.25 μg/mL], and one potently synergizes with methicillin (fractional inhibitory concentration index = 0.25) and is protective in a mouse infection model. These results provide numerous leads for antibacterial development and open up the possibility of restoring sensitivity to drugs such as methicillin, using combination therapies.

drug discovery | *in silico* high-throughput screening | peptidoglycan | protein structure

Targeting isoprenoid biosynthesis is a potentially important route for antibiotic discovery because isoprenoids are involved in the very early steps of bacterial cell-wall biosynthesis—the condensation of dimethylallyl diphosphate (DMAPP, **1**) with two molecules of isopentenyl diphosphate (IPP, **2**) to form farnesyl diphosphate (FPP, **3**), catalyzed by the enzyme farnesyl diphosphate synthase (FPPS), followed by the addition of eight more IPP molecules to form undecaprenyl diphosphate (UPP, **4**) (1, 2) (Fig. 1). Formation of **4** is catalyzed by the enzyme undecaprenyl diphosphate synthase (UPPS), and several UPPS inhibitors have been reported (3–10). UPP is then hydrolyzed to the monophosphate, which is next converted to lipid I and lipid II, leading to formation of cell wall peptidoglycan (Fig. 1) (11, 12). Antibiotics such as methicillin and vancomycin act in the latter stages of peptidoglycan formation, again as shown in Fig. 1. Here, we focus on the development of UPPS inhibitors because UPPS is an essential protein not produced by humans (13). UPPS inhibitors are predicted to synergize with the more-conventional cell-wall biosynthesis inhibitors, potentially reducing the toxicity of drugs such as vancomycin (by decreasing dosage), or restoring drug sensitivity [e.g., with methicillin-resistant *Staphylococcus aureus* (MRSA)]. The UPPS structure is unusual in that there are four known ligand binding sites (5), opening up the possibility of designing a diverse range of inhibitors.

Results and Discussion

UPPS Inhibitors. In previous work, we and others reported the discovery of several UPPS inhibitors, including bisphosphonates such as BPH-629 (**5**) (5), tetramic acids such as **6** (6), as well as diketoacids such as **7** (10) and benzoic acids such as **8** (9) (Fig. 2). Based on *in silico* high-throughput screening (9) and hit development (Fig. S1), we produced a small series of benzoic (**9**–**12**), phosphonic (**13**), and diketoacids (**14**, **15**) that had activity against UPPS (Fig. 2). In addition to these anionic species, we discovered several potent cationic inhibitors (**16**–**18**); this was unexpected from both a computational and experimental standpoint because these compounds do not mimic the (anionic) FPP substrate, and the UPPS mechanism is not thought to involve carbocation intermediates (14). We thus sought to determine how these inhibitors bind to their UPPS target, by obtaining crystal structures of **8**–**16** and **18** bound to *Escherichia coli* UPPS.

Four Inhibitor Binding Sites in UPPS. UPPS functions by sequentially adding IPP to an allylic substrate, initially FPP (15). It might reasonably be expected, then, that anionic inhibitors with lipophilic side-chains would bind to the FPP substrate site, as shown in Fig. 3*A*, yellow (PDB ID code 1X06). However, in a second structure (PDB ID code 1V7U), two FPP molecules bind, one in the substrate site and the other in a second site at the "bottom" of the protein (Fig. 3*A*, green). Moreover, with the bisphosphonate inhibitor **5**, there are actually four binding sites (sites 1–4) (5) that can be occupied (Fig. 3*B*, cyan; PDB ID code 2E98) in which the side chains in each of the four inhibitor molecules occupy the large hydrophobic center of the protein that normally accommodates the C_{55} side chain in the UPP product. With the two less-active benzoic acid inhibitors, **8** and **9**, we find that only site 3 (Fig. 3*C*; PDB ID code 3SGT) or sites 1, 2, and 3 are occupied (Fig. 3*D*; PDB ID code 3SGV), but the activity of both of these inhibitors is weak (**8**, *E. coli* UPPS, IC_{50} = 150 μM; *S. aureus* UPPS, 170 μM; **9**, *E. coli* UPPS, IC_{50} = 35 μM, *S. aureus* UPPS, 72 μM; Table S1). Full data acquisition and structure refinement details are in Table S2, and electron densities (2Fo-Fc and simulated-annealing Fo-Fc omit maps) are in Fig. S2 *A* and *B*. So, with these two benzoic acid inhibitors, binding to sites 1, 2, or 3 correlates only to weak UPPS inhibition.

Potent Benzoic Acid Inhibitors Bind to Site 4. We next determined the structures of the three potent benzoic acid inhibitors (10–12) (Fig. 2) bound to UPPS (Fig. 4 *A*–*C*). Each of these molecules contains a long hydrophobic side-chain and, on average,

Author contributions: W.Z., Y.Z., J.A.M., and E.O. designed research; W.Z., Y.Z., W.S., M.E.H., J.O., K.J.M., S.L., R.C., K.L., K.W., Y.W., Y.-L.L., A.S., C.A.F.d.O., D.A.M., V.N., J.A.M., and E.O. performed research; and E.O. wrote the paper.

The authors declare no conflict of interest.

Data deposition: Crystallography, atomic coordinates, and structure factors have been deposited in the Protein Data Bank, www.pdb.org (PDB ID codes 3SGT, 3SGV, 3SGX, 3SH0, 4H2O, 4H38, 4H3C, 4H3A, 4H2J, 4H2M, and 4H8E).

[1]W.Z., Y.Z., and W.S. contributed equally to this work.

[2]To whom correspondence may be addressed. E-mail: eo@chad.scs.uiuc.edu, yhzhang@illinois.edu, or jmccammon@ucsd.edu.

This article contains supporting information online at www.pnas.org/lookup/suppl/doi:10.1073/pnas.1219899110/-/DCSupplemental.

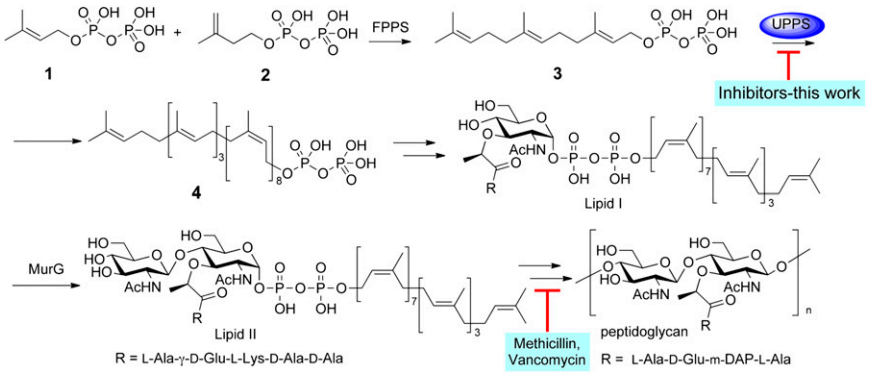

Fig. 1. Schematic outline of cell wall biosynthesis (in most bacteria) showing involvement of isoprenoid biosynthesis in the early stages of peptidoglycan formation.

the IC_{50} values against both *E. coli* and *S. aureus* UPPS are ~3 μM (Table S1). What is notable about these X-ray structures is that in each case, site 4 is occupied, together with either sites 1, 2, or 3. Full data acquisition and structure refinement details are in Table S2, and electron densities are in Fig. S2 *A* and *B*. In addition, we found that the aryl phosphonate inhibitor **13** also occupied two sites (Fig. 4*D*). However, there are two chains in one asymmetric unit, and site occupancies in the two chains are variable: the lower site-occupancy chains are shown in Fig. S2*C*. These four structures suggest that good UPPS inhibition correlates with occupancy of site 4.

Diketoacids, a Bisamidine and a Bisamine also Target Site 4. In previous work (10), we found that the diketoacid **15** had potent cell-growth inhibition activity with the following minimal inhibitory concentration $(MIC)_{90}$ values: 0.25–0.5 μg/mL against *S. aureus*; 0.5 μg/mL against *Bacillus anthracis*; 4 μg/mL against *Listeria monocytogenes* and *Enterococcus faecium*; and 1 μg/mL against *Streptococcus pyogenes*, but little toxicity toward human cell lines (>20 μM). We therefore determined the structure of **15** and a second diketoacid (**14**), bound to UPPS. As seen in Fig. 5 *A* and *B*, both diketoacids bind to site 4, with **14** also binding to site 3. The observation that **15** binds only to site 4 is of interest because this inhibitor has very good antibiotic activity (10). Plus, the occupation of site 4 in both structures is consistent with the results for the other potent anionic inhibitors (Fig. 4).

A surprising result from the *in silico* screening work (Fig. S1) was that bisamidines such as **16** had modest activity against UPPS. Moreover, the biphenyl bisamidine **17** showed potent activity against UPPS (IC_{50} = 0.1 μM) as well as a MIC_{90} of 0.25 μg/mL against *S. aureus* (USA300, MRSA strain). We also found that another dicationic species **18** was a UPPS inhibitor active against *S. aureus* (Table S1). We were unable to obtain the structure of **17** bound to UPPS, but we did obtain structures of **16** and **18** bound to UPPS.

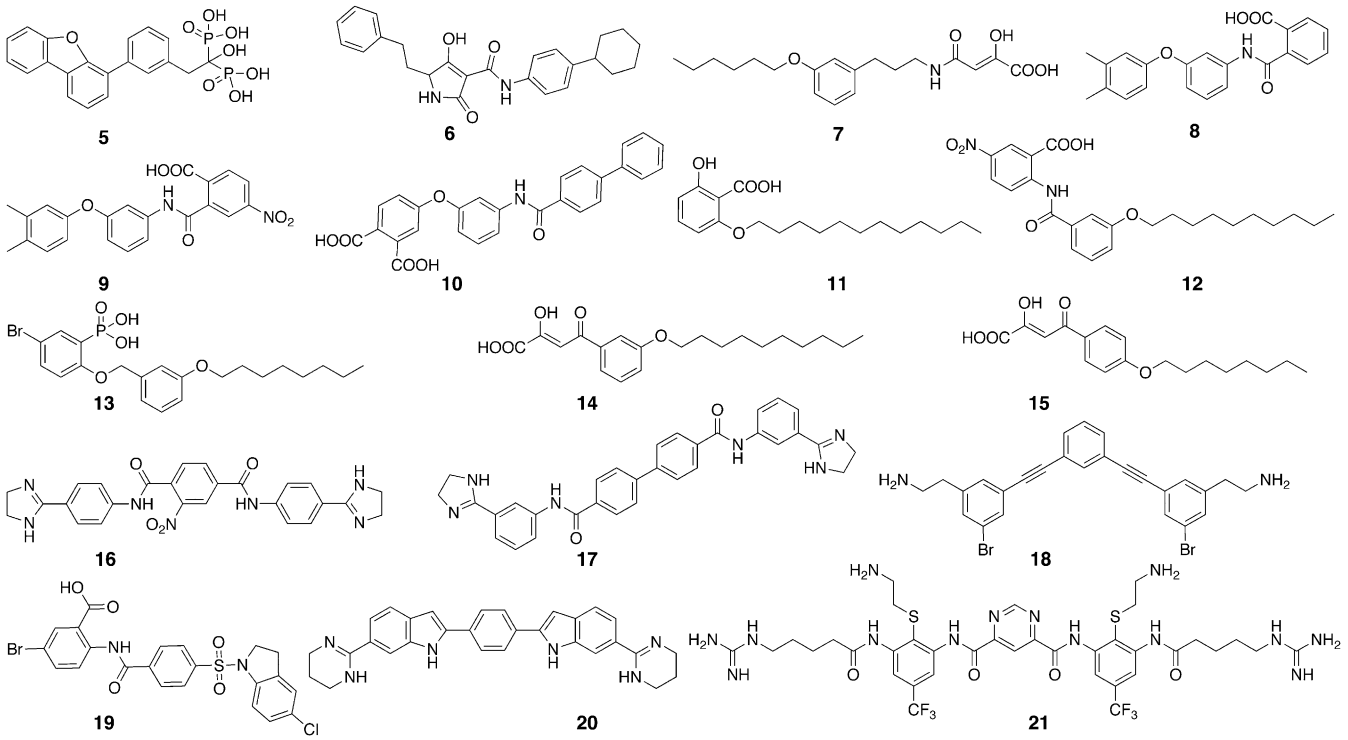

Fig. 2. Chemical structures of UPPS inhibitors and drug leads of interest.

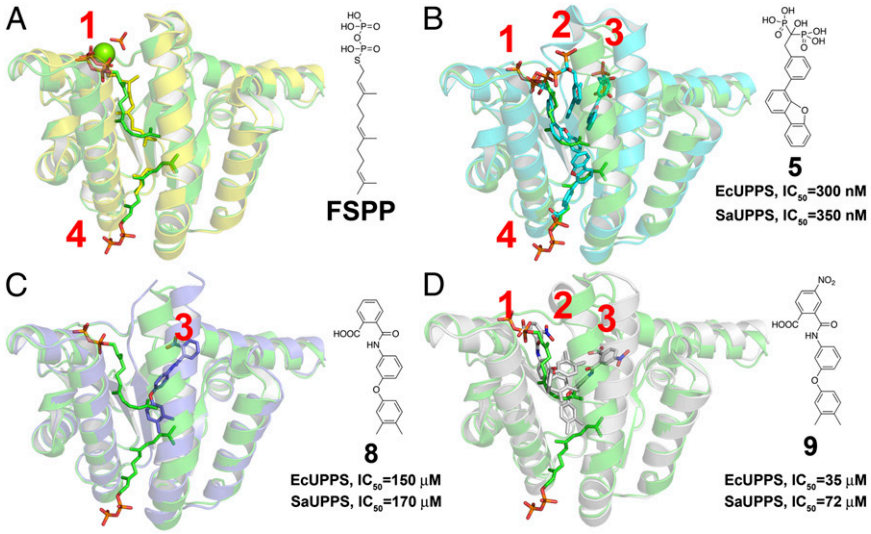

Fig. 3. X-ray structures of *E. coli* UPPS showing substrate and inhibitor binding sites. (*A*) FSPP (yellow) binds to site 1 (PDB ID code 1X06) and FPP (green) binds to sites 1 and 4 (PDB ID code 1V7U). (*B*) A bisphosphonate (**5**) binds to sites 1–4 (PDB ID code 2E98). (*C*) Benzoic acid inhibitor **8** binds to site 3 (cyan, PDB ID code 3SGT), superimposed on FPP-bound structure (green, PDB ID code 1V7U). (*D*) Benzoic acid inhibitor **9** binds to sites 1–3 (cyan, PDB ID code 3SGV), superimposed on FPP-bound structure (green, PDB ID code 1V7U). The large red numbers indicate sites 1–4.

With these two cationic inhibitors, rather than two individual molecules binding, we observe that a single molecule binds, with its polar, cationic groups located at or near the protein's surface, whereas the hydrophobic "spacer" is buried inside the protein's hydrophobic interior, (Fig. 5 *C* and *D*; PDB ID codes 4H2J and 4H2M). Though we did not succeed in crystallizing the most potent lead **17**, a similar "polar-hydrophobic-polar" binding arrangement in which the biphenyl group is buried seems very likely for this species also, and is supported by the results of computational docking, as shown in Fig. S2*D*.

Comparison of *E. coli* and *S. aureus* UPPS Structures and Their Inhibition. In this work, we determined the activity of each inhibitor against both *E. coli* UPPS and *S. aureus* UPPS, finding that there is a very good correlation ($R^2 = 0.8$) between the 14 sets of pIC_{50} ($= -\log_{10}IC_{50}$) values (Table S1; Fig. S3*A*); this is not unexpected because 18 of the top 20 residues in a SCORECONS (16) analysis of *E. coli* UPPS are present in *S. aureus* UPPS and most other bacterial UPPSs (Table S3). We were not able to determine the X-ray structures of any inhibitor bound to *S. aureus* UPPS, but we did determine the structure of the protein with a bound FPP (PDB ID code 4H8E; full data acquisition and structure refinement details are in Table S4). *S. aureus* UPPS cocrystallized with FPP in site 1, together with a SO_4^{2-} in the IPP binding site, as reported in a patent application (17). A superposition of the *S. aureus* and *E. coli* proteins is shown in Fig. S3*B*, where we find a Cα rmsd of 0.91 Å over 202 residues, indicating that both structures are very similar [in the presence of FPP/FSPP (*S-thiolo*-FPP) and either IPP or SO_4^{2-}], consistent with the pIC_{50} correlation.

Relationship to Other Inhibitors: Is UPPS a Missing Link? The structures of several of the UPPS inhibitors described here are similar to (and with **18**, the same as) those being developed as antiinfective drug leads but whose mechanisms of action are not clear. For example, the chemical structures of the benzoic acid inhibitors are similar to those of anthranilic (*ortho*-aminobenzoic) acids reported by Larsen et al. (18) and Mott et al. (19) having activity against *S. aureus*. The molecular mechanism of action of these inhibitors was initially thought to involve inhibition of translation/termination, but in later work this inhibition was not found to correlate with cell growth inhibition, and a new target (SA1575, of unknown function), as well as inhibition of cell wall biosynthesis, was reported. We find that

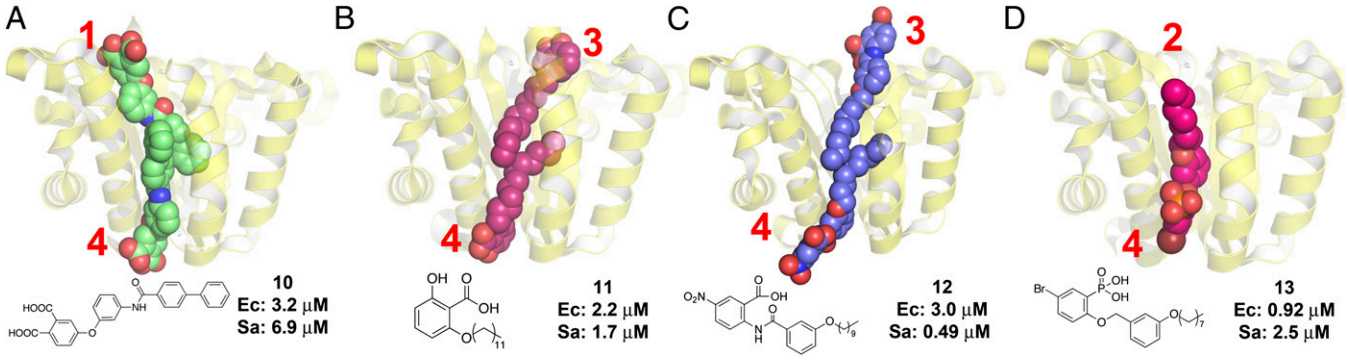

Fig. 4. Crystal structures of the more potent benzoic acids and a phosphonate inhibitor. (*A*) **10** (PDB ID code 3SGX). (*B*) **11** (PDB ID code 3SH0). (*C*) **12** (PDB ID code 4H2O). (*D*) **13** (PDB ID code 4H38). In each case, site 4 is occupied, together with either site 1, 2, or 3, indicating the likely importance of site 4 binding for good activity. The values shown are the IC_{50}s for *E. coli* UPPS inhibition (Ec) or *S. aureus* UPPS inhibition (Sa).

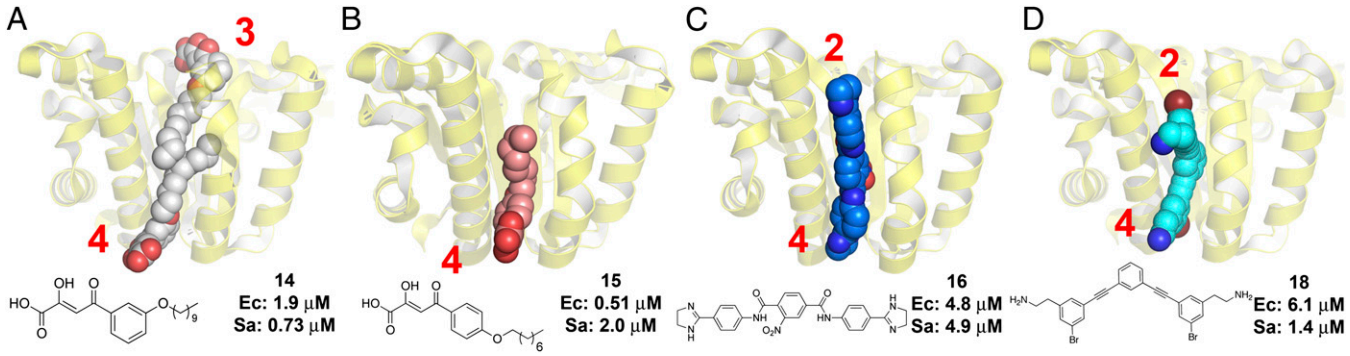

Fig. 5. Crystal structures of diketo acids and two dicationic inhibitors bound to *E. coli* UPPS. (*A*) **14** (PDB ID code 4H3C). (*B*) **15** (PDB ID code 4H3A). (*C*) **16** (PDB ID code 4H2J). (*D*) **18** (PDB ID code 4H2M). The common feature in each case is binding to site 4. The values shown are the IC_{50}s for *E. coli* UPPS inhibition (Ec) or *S. aureus* UPPS inhibition (Sa).

a pharmacophore model (Fig. 6*A*) of seven potent benzoic acid UPPS inhibitors we synthesized (Fig. S4*A*) is very similar to that obtained for *S. aureus* cell growth inhibition (Fig. 6*B*) using five structures reported by Larsen et al. (Fig. S4*B*), making UPPS inhibition one likely mechanism for these inhibitors—in particular because they are already known to inhibit cell wall biosynthesis. In addition, we found that the lead **19** reported by Larsen et al. (18) is a ~1 to 2 μM UPPS inhibitor (Table S1), consistent with a role in *S. aureus* growth inhibition.

In addition to the benzoic/anthranilic acids, there is also interest in the mechanisms of action of bisamidines, such as **20** (20, 21), as well as of other cationic species, such as **21** (22), and it has been proposed that these and related compounds could bind to the minor groove of DNA (20), or that they could alter lipid bilayer structure (23–25), as illustrated schematically in Fig. 6 *C* and *D*. Based on our crystallographic (Fig. 5 *C* and *D*) as well as enzyme inhibition results, it is clear, however, that in addition to these binding modes, polar-hydrophobic-polar inhibitors (such as **17** or **18**) can also bind to proteins, as shown in the cartoon in Fig. 6*E*, with their polar headgroups located near polar protein residues (or at the protein/water interface), whereas their hydrophobic centers are buried inside the protein target (Fig. 5 *C* and *D*).

Notably, as with the benzoic acids, bisamidines such as **20** can inhibit cell wall biosynthesis, and with **20** we find quite potent (470 nM) UPPS inhibition.* The ability to inhibit UPPS in addition to, e.g., DNA and lipid membrane targeting likely contribute to the potent activity of these compounds and, in some cases, the lack of resistance observed experimentally. In addition, it is also possible that other prenyltransferases, such as FPPS, may in some cases be targeted.

Synergy and in Vivo Results. The UPPS inhibition results suggested to us the possibility of synergistic activity with downstream cell-wall biosynthesis inhibitors, such as methicillin (Fig. 1); this is indeed the case, as shown in Fig. 7*A* in which we present the isobologram (26) for **17** + methicillin against a USA300 strain of MRSA. We observe a potent synergistic interaction with a fractional inhibitory concentration index (FICI), defined as

$$\mathrm{FICI} = \mathrm{FIC_A} + \mathrm{FIC_B} = \mathrm{MIC_{90}(AB)/MIC_{90}(A)} + \mathrm{MIC_{90}(BA)/MIC_{90}(B)},$$

where, $\mathrm{FIC_A}$, $\mathrm{FIC_B}$ are the fractional inhibitory concentrations of drugs A and B, and $\mathrm{MIC_{90}}$ (AB), $\mathrm{MIC_{90}}$ (BA) are the $\mathrm{MIC_{90}}$ values of the most effective combination of A or B in the presence of B or A (27, 28). Using this method, FICI values <0.5 represent synergism; >0.5 and <1.0 represent additivity; >1 and <2 represent an indifferent effect; and ≥2 represents drug antagonism (29). An FICI = 0.25 thus represents strong synergism, opening up the probability of restoring drug sensitivity in drug-resistant strains. However, are such compounds active in in vivo models of infection?

In previous work, it has been found that, e.g., benzoic acids (such as **19**) as well as tetramic acids (such as **6**) have potent activity against bacteria; however, there have been no previous

*Opperman TJ, et al. Poster Session, 50th Interscience Conference on Antimicrobial Agents and Chemotherapy, September 12–15, 2010, Boston.

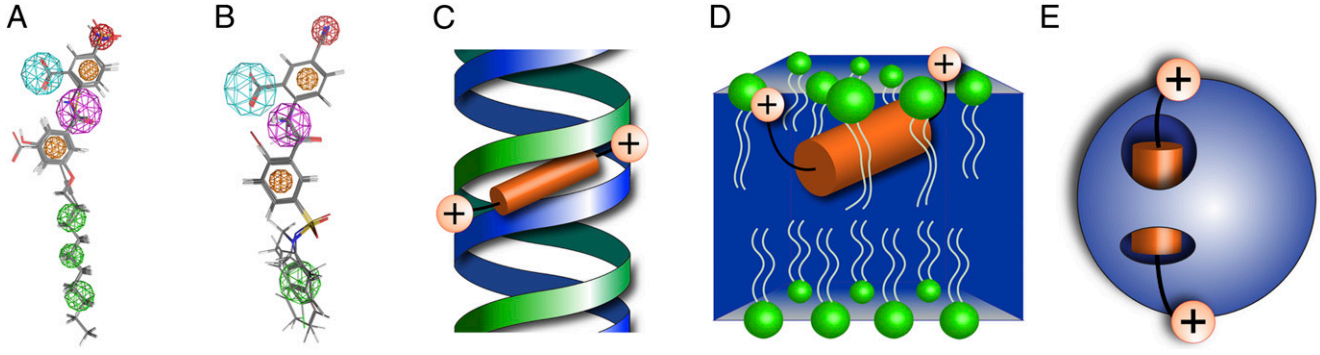

Fig. 6. UPPS as a missing link. Models and cartoons. (*A*) Pharmacophore model for UPPS inhibition by benzoic acids. (*B*) Pharmacophore model for *S. aureus* growth inhibition by benzoic acids. Common features are benzoic acid carboxylates (cyan) with electron-withdrawing *meta* substituents (red); an x–y spacer (dark pink); two aromatic features (orange); and more-distal hydrophobic features (green). (*C*) Cationic-hydrophobic-cationic inhibitor binding to DNA. (*D*) Cationic-hydrophobic-cationic inhibitor binding to anionic lipids in a membrane. (*E*) Cationic-hydrophobic-cationic inhibitor binding to a protein.

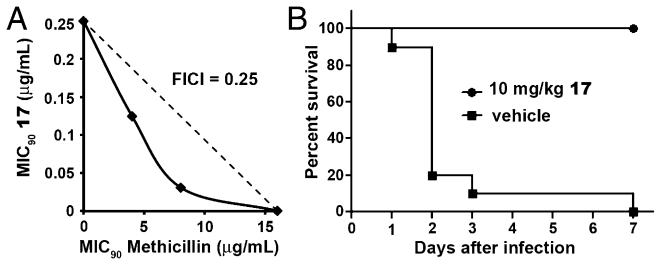

Fig. 7. In vitro synergy and in vivo results with **17**. (*A*) Isobologram for **17** + methicillin inhibition of *S. aureus* (USA300) cell growth. FICI = 0.25. (*B*) Activity of **17** in a mouse model of *S. aureus* (USA200) infection. Shown is one representative experiment repeated twice (n = 10 mice per group per experiment). No mice in the group treated once daily with 10 mg/kg of **17** (three doses total) died during either experiment.

reports of in vivo activity, due perhaps to strong binding to plasma proteins. Because **17** had potent activity against UPPS (110 nM), we tested it in a mouse model of infection using the USA200 Sanger 252 (MRSA) strain of *S. aureus*. As can be seen in Fig. 7*B*, mice treated postinfection only with vehicle control all died, whereas mice treated with **17** (20/20 total, pooled results of two experiments) survived with no apparent adverse reactions.

Computational Results: FTMap, Principal Component, and Receiver Operating Characteristic/Area Under the Curve Analyses. The results described above represent the discovery of a series of UPPS inhibitors—drug leads—some of which have potent activity in cells and a mouse infection model. From a structural perspective, the most surprising result was that the most potent inhibitors all bound to site 4, not the substrate site, site 1. In previous work on bisphosphonate UPPS inhibitors (5) we found that a wide range of bisphosphonates bound to site 1, and that enzyme inhibition and site 1 docking scores were highly correlated (5). However, with all of the nonbisphosphonate inhibitors described here, we find that binding to site 4 is the common structural denominator for ligands with high affinity. Other sites are also often occupied, with either two molecules binding, or one inhibitor spanning two sites (sites 4 and 2, with the dicationic species).

Site 4 is quite removed from the most-flexible loop region (residues 72–82) of the active site, suggesting that there may be fewer entropic costs due to constraining this loop, associated with inhibitor binding to site 4, rather than to sites 1–3, where the ligand directly contacts and restrains the loop. Site 4 is also predicted to be druggable when using the solvent-mapping program FTMap (30), as shown in Fig. 8*A*, again supporting the idea that inhibitors that bind to site 4 will be good drug leads. With the nonbisphosphonate inhibitors, we also see that the global structures are quite similar to apo UPPS (Fig. 8*B*, red), using principal component analysis (31). The bisphosphonate inhibitors (blue) and substrate (yellow)-bound structures are altered to a greater extent from the apo form than are the nonbisphosphonate structures (red), which suggests less induced-fit occurs on binding, which again will reduce any energetic costs associated with protein conformational changes upon binding.

Finally, because many of these inhibitors were the result of virtual screening, we assessed the predictive nature of each structure using a receiver operating characteristic/area under the curve (ROC/AUC) approach (32) with a 112-compound screening dataset (Fig. S5). Enrichment results are shown in Fig. 8*C* and Fig. S6. Good results (AUC = 0.768) are obtained when using the "open" structure containing **5** bound to sites 1–4, but the best result is obtained using the **15** structure (PDB ID code 4H3A), an "ajar" (Fig. 8*B*) or partially closed structure in which only site 4 is occupied (Fig. 8*C*, bottom), where AUC = 0.802. Taken together, these results strongly support the importance of developing compounds that bind to site 4 as UPPS inhibitor drug leads, and that computational models based on these structures can significantly enrich the hit rate.

Conclusions

The results we have described herein are of interest for several reasons. First, we obtained the X-ray structures of 10 UPPS inhibitors covering a diverse range of structures: benzoic acids, diketoacids, an aryl phosphonate, a bisamidine, and a bisamine. The surprising result was that both cationic as well as anionic compounds were inhibitors, the cationic species having an unusual polar-hydrophobic-polar structural motif. Second, we find evidence that occupancy of site 4 (not the FPP substrate site, site 1) correlates with the potent activity of these inhibitors, and that site 4 is predicted to be druggable. Third, we find that the cationic

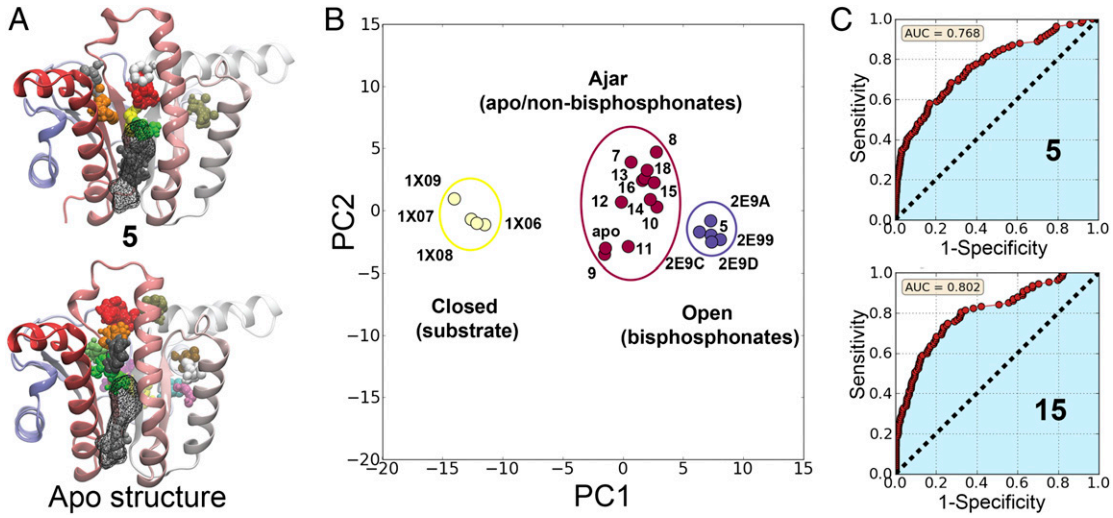

Fig. 8. Computational analysis of UPPS structural results. (*A*) FTMap computational solvent mapping of UPPS structures (PDB ID codes 2E98 and 3QAS) suggest that site 4 is druggable in either inhibitor-bound complexes or unbound. UPPS is represented as a cartoon; small probes are colored spheres; black wireframe outlines site 4. (*B*) Principal component analysis of *E. coli* UPPS structures. Substrate-bound structures (yellow) are closed (33); bisphosphonates (blue) are open (33); the apo and nonbisphosphonate structures (red) are all ajar (slightly open). (*C*) ROC/AUC analysis of most-predictive UPPS structures in terms of initial enrichment for actives under 100 μM (Fig. S6).

(bisamidine and a bisamine) inhibitors span both sites 2 and 4, with their polar groups at or near the protein/water interface, whereas their hydrophobic domains are buried. This result is of particular importance because this motif is very similar to that proposed to be important for DNA and lipid membrane binding with structurally related inhibitors, leading to the idea that such compounds may have multiple targets (including UPPS), thereby increasing potency. We also find that a closely related biphenyl analog (**17**) inhibits UPPS at ~100 nM levels, has a MIC_{90} of 0.25 μg/mL, and strongly synergistic activity (FICI = 0.25) with methicillin in an MRSA strain otherwise resistant to the antibiotic. In addition, this compound shows clear therapeutic activity in a mouse model of infection. Finally, we propose that anthranilic acids, known to be potent inhibitors of *S. aureus* growth that target cell-wall biosynthesis, also target bacterial UPPS. Taken together, these results open up additional routes to anti-infective therapies targeting bacterial isoprenoid biosynthesis, and suggest that in some cases drug leads that have been proposed to target DNA and lipid membrane structure may also target bacterial cell-wall biosynthesis via UPPS inhibition.

Methods

E. coli UPPS and *S. aureus* UPPS were expressed and purified as described previously (9). UPPS inhibition assays were carried out as described previously (5). UPPS/inhibitor crystals were obtained via soaking as described previously (5). Structure determinations and refinements were carried out basically as described previously (5), with full details given in *SI Methods*. For the 11 structures reported, the resolution was on average 1.88 Å (±0.29 Å), and R_{free} was on average 24.6% (±3.9%). Full synthesis and characterization details for all compounds investigated crystallographically are provided in *SI Methods*. In vivo experiments used female BALB/c mice infected intraperitoneally with *S. aureus* (USA200), as described in detail in *SI Methods*. Bacterial cell-growth inhibition assays were carried out as described previously (10). The care and experimental manipulation of our mice were reviewed and approved by the Institutional Animal Care and Use Committee at the University of California at San Diego.

ACKNOWLEDGMENTS. We thank Yigui Gao from the University of Illinois Macromolecular Crystallization Laboratory for providing crystallization facilities, and F. Guerra for help with the graphics. Use of the Advanced Photon Source was supported by the US Department of Energy, Office of Science, Office of Basic Energy Sciences, under Contract DE-AC02-06CH11357. Use of the Life Science Collaborative Access Team Sector 21 was supported by the Michigan Economic Development Corporation and Michigan Technology Tri-Corridor Grant 085P1000817. Funding for this work was provided by US Public Health Services National Institutes of Health (NIH) Grants AI074233, GM65307, and CA158191. Work at the University of California at San Diego was supported by Molecular Biophysics Training Grant GM08326; NIH Grants GM31749 and HD071600; National Science Foundation Grant MCB-1020765; the National Biomedical Computation Resource, the Center for Theoretical Biological Physics, and the Howard Hughes Medical Institute.

1. Oldfield E (2010) Targeting isoprenoid biosynthesis for drug discovery: Bench to bedside. *Acc Chem Res* 43(9):1216–1226.
2. Oldfield E, Lin FY (2012) Terpene biosynthesis: Modularity rules. *Angew Chem Int Ed Engl* 51(5):1124–1137.
3. Scholte AA, Eubanks LM, Poulter CD, Vederas JC (2004) Synthesis and biological activity of isopentenyl diphosphate analogues. *Bioorg Med Chem* 12(4):763–770.
4. Guo RT, et al. (2005) Crystal structures of undecaprenyl pyrophosphate synthase in complex with magnesium, isopentenyl pyrophosphate, and farnesyl thiopyrophosphate: Roles of the metal ion and conserved residues in catalysis. *J Biol Chem* 280(21):20762–20774.
5. Guo RT, et al. (2007) Bisphosphonates target multiple sites in both *cis*- and *trans*-prenyltransferases. *Proc Natl Acad Sci USA* 104(24):10022–10027.
6. Peukert S, et al. (2008) Design and structure-activity relationships of potent and selective inhibitors of undecaprenyl pyrophosphate synthase (UPPS): Tetramic, tetronic acids and dihydropyridin-2-ones. *Bioorg Med Chem Lett* 18(6):1840–1844.
7. Fujikura K, Maki Y, Ohya N, Satoh M, Koyama T (2008) Kinetic studies of *Micrococcus luteus* B-P 26 undecaprenyl diphosphate synthase reaction using 3-desmethyl allylic substrate analogs. *Biosci Biotechnol Biochem* 72(3):851–855.
8. Kuo CJ, et al. (2008) Structure-based inhibitors exhibit differential activities against *Helicobacter pylori* and *Escherichia coli* undecaprenyl pyrophosphate synthases. *J Biomed Biotechnol* 2008:841312.
9. Durrant JD, et al. (2011) Non-bisphosphonate inhibitors of isoprenoid biosynthesis identified via computer-aided drug design. *Chem Biol Drug Des* 78(3):323–332.
10. Zhang Y, et al. (2012) HIV-1 integrase inhibitor-inspired antibacterials targeting isoprenoid biosynthesis. *ACS Med Chem Lett* 3(5):402–406.
11. van Heijenoort J (2007) Lipid intermediates in the biosynthesis of bacterial peptidoglycan. *Microbiol Mol Biol Rev* 71(4):620–635.
12. Hao H, Cheng G, Dai M, Wu Q, Yuan Z (2012) Inhibitors targeting on cell wall biosynthesis pathway of MRSA. *Mol Biosyst* 8(11):2828–2838.
13. Apfel CM, Takács B, Fountoulakis M, Stieger M, Keck W (1999) Use of genomics to identify bacterial undecaprenyl pyrophosphate synthetase: Cloning, expression, and characterization of the essential uppS gene. *J Bacteriol* 181(2):483–492.
14. Lu YP, Liu HG, Liang PH (2009) Different reaction mechanisms for *cis*- and *trans*-prenyltransferases. *Biochem Biophys Res Commun* 379(2):351–355.
15. Lu YP, Liu HG, Teng KH, Liang PH (2010) Mechanism of *cis*-prenyltransferase reaction probed by substrate analogues. *Biochem Biophys Res Commun* 400(4):758–762.
16. Valdar WSJ (2002) Scoring residue conservation. *Proteins* 48(2):227–241.
17. Ammirati M, Pandit J (2002) Crystal structure of *Staphylococcus* undecaprenyl pyrophosphate synthase and uses thereof. US Patent Application No. 10/688,167.
18. Larsen SD, et al. (2006) Discovery and initial development of a novel class of antibacterials: Inhibitors of *Staphylococcus aureus* transcription/translation. *Bioorg Med Chem Lett* 16(24):6173–6177.
19. Mott JE, et al. (2008) Resistance mapping and mode of action of a novel class of antibacterial anthranilic acids: Evidence for disruption of cell wall biosynthesis. *J Antimicrob Chemother* 62(4):720–729.
20. Panchal RG, et al. (2009) Novel broad-spectrum bis-(imidazolinylindole) derivatives with potent antibacterial activities against antibiotic-resistant strains. *Antimicrob Agents Chemother* 53(10):4283–4291.
21. Butler MM, et al. (2010) Comparative in vitro activity profiles of novel bis-indole antibacterials against gram-positive and gram-negative clinical isolates. *Antimicrob Agents Chemother* 54(9):3974–3977.
22. Tew GN, Scott RW, Klein ML, Degrado WF (2010) De novo design of antimicrobial polymers, foldamers, and small molecules: From discovery to practical applications. *Acc Chem Res* 43(1):30–39.
23. Som A, Tew GN (2008) Influence of lipid composition on membrane activity of antimicrobial phenylene ethynylene oligomers. *J Phys Chem B* 112(11):3495–3502.
24. Su Y, DeGrado WF, Hong M (2010) Orientation, dynamics, and lipid interaction of an antimicrobial arylamide investigated by 19F and 31P solid-state NMR spectroscopy. *J Am Chem Soc* 132(26):9197–9205.
25. Yang L, et al. (2008) Mechanism of a prototypical synthetic membrane-active antimicrobial: Efficient hole-punching via interaction with negative intrinsic curvature lipids. *Proc Natl Acad Sci USA* 105(52):20595–20600.
26. Berenbaum MC (1989) What is synergy? *Pharmacol Rev* 41(2):93–141.
27. Eliopoulos GM, Moellering RC (1998) Antimicrobial combinations. *Antibiotics in Laboratory Medicine*, ed Lorian V (Williams & Wilkins, Baltimore), 4th Ed, pp 330–396.
28. Singh PK, Tack BF, McCray PB, Jr., Welsh MJ (2000) Synergistic and additive killing by antimicrobial factors found in human airway surface liquid. *Am J Physiol Lung Cell Mol Physiol* 279(5):L799–L805.
29. European Committee for Antimicrobial Susceptibility Testing (EUCAST) of the European Society of Clinical Microbiology and Infectious Dieases (ESCMID) (2000) EUCAST Definitive Document E.Def 1.2, May 2000: Terminology relating to methods for the determination of susceptibility of bacteria to antimicrobial agents. *Clin Microbiol Infect* 6(9):503–508.
30. Ngan CH, et al. (2012) FTMap: Extended protein mapping with user-selected probe molecules. *Nucleic Acids Res* 40(Web Server issue):W271–W275.
31. Grant BJ, Rodrigues APC, ElSawy KM, McCammon JA, Caves LSD (2006) Bio3d: An R package for the comparative analysis of protein structures. *Bioinformatics* 22(21):2695–2696.
32. Lee HS, et al. (2008) Optimization of high throughput virtual screening by combining shape-matching and docking methods. *J Chem Inf Model* 48(3):489–497.
33. Teng KH, Liang PH (2012) Structures, mechanisms and inhibitors of undecaprenyl diphosphate synthase: A *cis*-prenyltransferase for bacterial peptidoglycan biosynthesis. *Bioorg Chem* 43:51–57.

Supporting Information

Zhu et al. 10.1073/pnas.1219899110

SI Methods

Synthetic Aspects. All reagents used were purchased from Aldrich or Alfa Aesar. NMR spectra were obtained on 400 MHz (^{1}H) or 500 MHz Varian Unity spectrometers. Chemical shifts are reported in parts per million (ppm) using tetramethylsilane as an external standard using the convention that high frequency, low field, paramagnetic or de-shielded values are positive. The structures **10**, **14**, and **15** were available from previous work (1, 2). The syntheses of **11**, **12**, **13**, **16**, **17**, and **18** are described below.

(Dodecyloxy)-6-Hydroxybenzoic Acid (11). To a mixture of 5-hydroxy-2, 2-dimethyl-4H-benzo[d][1,3]dioxin-4-one (1 g, 5.2 mmol) and 1-dodecanol (1.6 g, 7.5 mmol) in tetrahydrofuran (THF) (20 mL) at 0 °C were added triphenyl phosphine (2.0 g, 7.5 mmol) and diisopropyl azodicarboxylate (DIAD) (1.5 mL, 7.5 mmol). The mixture was then stirred overnight at room temperature. The reaction mixture was concentrated and purified by column chromatography [ethyl acetate/hexane 1:8 (vol/vol)]. Saponification with 4 M NaOH (5 equivalent) under reflux and acidification with 1 M HCl afforded **11** as a white solid (1.07 g, 70% yield). ^{1}H NMR ($CDCl_3$, 500 MHz) δ: 7.36 (t, J = 8.5 Hz, 1 H), 6.68 (d, J = 8.5 Hz, 1 H), 6.45 (d, J = 8.5 Hz, 1 H), 4.20 (t, J = 6.5 Hz, 2 H), 1.91–1.87 (m, 2 H), 1.47–1.43 (m, 2 H), 1.28–1.24 (m, 16 H), 0.86 (t, J = 6.5 Hz, 3 H) ppm. ^{13}C NMR ($CDCl_3$, 125 MHz) δ: 171.2, 164.5, 158.3, 135.8, 130.3, 112.4, 102.4, 71.0, 32.1, 29.8, 29.7, 29.7, 29.6, 29.5, 29.40, 29.1, 26.1, 22.9, 14.4. High-resolution MS (HRMS) [ESI (electrospray ionization)]: m/z $[M + H]^+$ calculated for $C_{19}H_{31}O_4$ 323.2222, found 323.2231.

2-(3-(Decyloxy)Benzamido)-5-Nitrobenzoic Acid (12). To a mixture of 3-(decyloxy)benzoyl chloride (296 mg, 1 mmol) and 2-amino-5-nitrobenzoic acid (182 mg, 1 mmol) in CH_2Cl_2 (20 mL) was added Et_3N (1 mL). The mixture was stirred overnight and washed with water (5 mL) and 1 M HCl (4 mL) and then concentrated. Recrystallization from ethyl acetate/hexane 1:1 afforded **12** as white powder (185 mg, 42%). ^{1}H NMR ($CDCl_3$, 500 MHz) δ: 12.17 (s, 1 H), 9.16 (d, J = 9.5 Hz, 1 H), 9.03 (d, J = 3.0 Hz, 1 H), 8.47 (dd, J = 9.5, 3.0 Hz, 1 H), 7.54 (d, J = 1.0 Hz, 1 H), 7.53 (d, J = 8.0 Hz, 1 H), 7.42 (t, J = 8.0 Hz, 1 H), 7.13 (dd, J = 8.0, 1.0 Hz, 1 H), 4.03 (t, J = 6.5 Hz, 2 H), 1.82–1.78 (m, 2 H), 1.47–1.43 (m, 2 H), 1.26–1.22 (m, 12 H), 0.86 (t, J = 7.0 Hz, 3 H). ^{13}C NMR ($CDCl_3$, 125 MHz) δ: 169.6, 160.0, 147.6, 142.1, 135.3, 130.5, 130.3, 128.0, 121.0, 120.1, 119.3, 114.2, 113.6, 68.6, 32.1, 29.80, 29.8, 29.6, 29.5, 29.4, 26.6, 22.9, 14.3. HRMS (ESI): m/z $[M + H]^+$ calculated for $C_{24}H_{31}N_2O_6$ 443.2182; found 443.2174.

(5-Bromo-2-((3-(Octyloxy)Benzyl)Oxy)Phenyl)Phosphonic Acid (13). To a mixture of diethyl (5-bromo-2-hydroxyphenyl)phosphonate (1.54 g, 5.0 mmol) and 3-octyloxybenzyl alcohol (1.2 g, 5.0 mmol) in THF (20 mL) at 0 °C were added triphenyl phosphine (2.0 g, 7.5 mmol) and DIAD (1.5 mL, 7.5 mmol). The mixture was then stirred overnight at room temperature. The reaction mixture was concentrated and purified by column chromatography (ethyl acetate/hexane 1:1). The diethyl ester of **13** was then treated with 8 equivalent of trimethylbromosilane in anhydrous CH_2Cl_2 (15 mL) overnight. After removal of the solvent, the concentrated oil was treated with 10 mL methanol to afford **13** as white solid (1.62 g, 68%, two steps). ^{1}H NMR (DMSO-D_6, 400 MHz) δ: 7.70 (dd, J = 14.8, 2.8 Hz, 1 H), 7.54 (dd, J = 8.8, 2.8 Hz, 1 H), 7.20 (t, J = 7.6 Hz, 1 H), 7.10 (s, 1 H), 6.99 (m, 1 H), 6.98 (m, 1 H), 6.77 (dd, J = 2.4, 8.0 Hz, 1 H), 5.16 (s, 2 H), 4.13 (t, J = 6.8 Hz, 2 H), 1.64–1.60 (m, 2 H), 1.36–1.32 (m, 2 H), 1.25–1.21 (m, 8 H), 0.81 (t, J = 6.8 Hz, 3 H) ppm. ^{13}C NMR (DMSO-D_6, 125 MHz) δ: 171.4, 159.4, 159.1, 139.0, 136.2, 130.1, 126.0, 124.6, 119.5, 115.9, 114.6, 113.3, 69.7, 60.6, 31.9, 31.3, 29.4, 29.3, 26.15, 22.7, 14.6. HRMS (ESI): m/z $[M + H]^+$ calculated for $C_{21}H_{29}BrO_5P$ 471.0936; found 471.0940.

N^1, N^4-Bis(3-(4,5-Dihydro-1H-Imidazol-2-yl)Phenyl)-2-Nitroterephthalamide (16). Structure **16** was obtained from the National Cancer Institute screening library, and its identity was confirmed by ^{1}H NMR, ^{13}C NMR, and HRMS. ^{1}H NMR (DMSO-D_6, 500 MHz) δ: 8.72 (s, 1 H), 8.44 (d, J = 7.5 Hz, 1 H), 7.99 (d, J = 7.5 Hz, 1 H), 7.90–7.81 (m, 6 H), 7.71 (d, J = 8.5 Hz, 2 H), 3.60 (s, 8 H). ^{13}C NMR (DMSO-D_6, 125 MHz) δ: 163.8, 163.5, 147.0, 141.0, 137.5, 135.0, 133.9, 130.5, 128.6, 128.4, 126.9, 124.2, 120.5, 119.7, 39.8. HRMS (ESI): m/z $[M + H]^+$ calculated for $C_{26}H_{24}N_7O_4$, 498.1890; found 498.1882.

N^4, $N^{4'}$-Bis(3-(4,5-Dihydro-1H-Imidazol-2-yl)Phenyl)-[1,1′-Biphenyl]-4,4′-Dicarboxamide (17). To a mixture of 4,4′-diphenyl dicarbonyl chloride (1.39 g, 5 mmol), 3-aminobenzonitrile (1.18 g, 10 mmol) in anhydrous THF (20 mL) was added Et_3N (2.1 mL, 15 mmol) and the mixture was stirred at room temperature overnight. After filtration, the white solid was washed with water (20 mL) and ethyl acetate (10 mL) and then dried. Sodium hydrosulfide hydrate (100 mg), ethylenediamine (2 mL), and dimethylacetamide (10 mL) were then added and stirred overnight at 140 °C. Upon removal of the solvent, the solid was washed thoroughly with water and then ethyl acetate (10 mL). To the suspension of the crude product in 10 mL of water were added two equivalents of methyl sulfonic acid. Removal of water afforded **17** as its methanesulfonic acid salt (1.44 g, 40%). ^{1}H NMR (DMSO-D_6, 500 MHz) δ: 10.68 (s, 2 H), 10.52 (s, 4 H), 8.50 (s, 2 H), 8.12 (d, J = 9.0 Hz, 4 H), 8.02–7.98 (m, 2 H), 7.96 (d, J = 9 Hz, 4 H), 7.68–7.58 (m, 4 H), 4.00 (s, 8 H), 2.36 (s, 6 H). ^{13}C NMR (DMSO-D_6, 125 MHz) δ: 166.1, 166.1, 143.0, 140.6, 134.4, 130.6, 129.2, 127.7, 127.0, 124.3, 123.5, 120.8, 45.3. HRMS (ESI): m/z $[M + H]^+$ calculated for $C_{32}H_{29}N_6O_2$ 529.2361, found 529.2352.

2,2′-((1,3-Phenylenebis(Ethyne-2,1-Diyl))Bis(3-Bromo-5,1-Phenylene)) Diethanamine (18). Structure **18** was synthesized as reported (3). ^{1}H NMR (DMSO-D_6, 500 MHz) δ: 7.66–7.42 (m, 10 H), 3.19 (t, J = 8.0 Hz,4 H), 2.95 (t, J = 8.0 Hz,4 H) ppm. ^{13}C NMR (DMSO-D_6, 125 MHz) δ: 158.8, 141.2, 135.6, 133.6, 133.2, 132.8, 131.7, 130.4, 124.9, 123.3, 122.6, 89.7, 40.8, 32.9. HRMS (ESI): m/z $[M + H]^+$ calculated for $C_{26}H_{23}Br_2N_2$, 521.0228; found 521.0214.

Experimental Aspects. E. coli *undecaprenyl diphosphate synthase expression and purification.* The *E. coli* undecaprenyl diphosphate synthase (UPPS) plasmid was provided by Andrew H.-J. Wang (Academia Sinica, Taiwan). The purification of UPPS from *E. coli* followed the published protocol with modifications (4). The plasmid was transformed into *E. coli* BL21 (DE3) cells (Novagen) for expression. A single transformant was grown overnight at 37 °C in LB medium containing 100 μg/mL ampicillin. The 50-mL overnight cultures were transferred to 2 L fresh LB medium containing 100 μg/mL ampicillin and allowed to grow to OD_{600} = 0.6 before induction with 1 mM isopropyl β-D-1-thiogalactopyranoside. The cultures were induced for 4 h at 37 °C and harvested by centrifugation. Cell pellets were suspended in 60 mL buffer [25 mM Tris·HCl (pH 7.5) and 150 mM NaCl], followed by pulse sonication. The lysate was centrifuged

and the cell debris discarded. For purification, the cell-free extract was loaded into a 20-mL Ni-NTA column pre-equilibrated with 25 mM Tris·HCl (pH 7.5) and 150 mM NaCl. The column was washed with 30 mM imidazole-containing buffer. The His-tagged UPPS was eluted with a 0–100% gradient buffer [25 mM Tris·HCl (pH 7.5), 150 mM NaCl, and 300 mM imidazole]. The protein solution was dialyzed against 3 × 2 L buffer [25 mM Tris·HCl (pH 7.5) and 150 mM NaCl]. The His-tagged UPPS was then digested with FXa protease to remove the His-tag. The solution was then loaded onto Ni-NTA. The UPPS in the flow-through [25 mM Tris·HCl (pH 7.5), 150 mM NaCl, and 30 mM imidazole] was pure, as evidenced by SDS/PAGE, and was dialyzed into buffer [25 mM Tris (pH 7.5) and 150 mM NaCl] for storage. The final concentration was determined by using a Bradford protein assay kit.

Staphylococcus aureus *UPPS expression and purification.* The gene encoding UPPS was amplified from a plasmid (1) containing the *S. aureus* UPPS gene. The forward primer was 5′ GTA TTG AGG GTC GCA TGT TTA AAA AGC TAA TAA ATA AAA AGA ACA C 3′, and the reverse primer was 5′ AGA GGA GAG TTA GAG CCC TAC TCC TCA CTC 3′. The amplified UPPS gene was purified and ligated into a pET-32 Xa/LIC vector (Novagen). The plasmid with the *S. aureus* UPPS gene was subsequently expressed in *Escherichia coli* BL21 (DE3) cells (Novagen). The protocol for expression and purification of *S. aureus* UPPS was the same as that for *E. coli* UPPS.

X-ray crystallography. Native *E. coli* UPPS crystals for use in soaking were obtained by using the hanging-drop method (Hampton Research) by mixing 1 μL of UPPS protein solution [~14 mg/mL UPPS in 25 mM Tris·HCl (pH 7.5) and 150 mM NaCl] with 1 μL of mother liquor [25 mM Tris·HCl (pH 7.5), 150 mM NaCl, and 5% PEG 2,000–4,000] and then equilibrating with 400 μL mother liquor at room temperature. Tetragonal crystals appeared in 2 d and were then soaked in a cryoprotectant solution [25 mM Tris·HCl (pH 7.5), 150 mM NaCl, 30% EG, and 5% PEG 35,000] containing 1–5 mM inhibitors for 1 d.

S. aureus UPPS crystals with farnesyl diphosphate (FPP) were obtained by using the hanging-drop method (Hampton Research) by mixing 1 μL of UPPS protein solution [~5 mg/mL UPPS in 1.5 mM $MgCl_2$, 1.5 mM FPP, 25 mM Tris·HCl (pH 7.5), and 150 mM NaCl] with 1 μL of mother liquor [100 mM MES sodium salt (pH 6.5), 200 mM $(NH_4)SO_4$, and 25% PEG monomethyl ether 5,000) and then equilibrating with 400 μL mother liquor at room temperature. Bipyramidal crystals appeared overnight.

X-ray diffraction data for both *E. coli* UPPS and *S. aureus* UPPS were collected at the Life Science Collaborative Access Team 21-ID-D (F or G) at the Advanced Photon Source of Argonne National Laboratory. Diffraction data were processed and scaled using the program HKL3000 (HKL Research Inc.) (5). The statistics for data collection are listed in Tables S2 and S4.

The structures of the UPPS complexes were determined using a model prepared from the UPPS/BPH-629 complex structure (PDB ID code 2E98) with ligands and solvent removed. Structure refinements were carried out using Refmac (6, 7), Phenix (8), and COOT (9). All structure figures were prepared with PyMOL (10).

UPPS inhibition assays. *E. coli* UPPS and *S. aureus* UPPS inhibition assays were carried out as described previously (1). Briefly, the condensation of FPP with isopentenyl diphosphate (IPP) catalyzed by UPPS was monitored by using a continuous spectrophotometric assay (11) in 96-well plates with 200-μL reaction mixtures containing 400 μM 7-methyl-6-thioguanosine (MESG), 350 μM IPP, 35 μM FPP, 25 mM Tris·HCl (pH 7.5), 0.01% Triton X-100, and 1 mM $MgCl_2$. The IC_{50} values were obtained by fitting the inhibition data to a standard rectangular hyperbolic dose–response function in GraphPad PRISM 4.0 software (GraphPad Software). The IC_{50} values for the most active hits were verified by radiometric assay (12) with 2.5 μM FPP, 25 μM [^{3}H]IPP, and 0.01% Triton X-100.

Computational Aspects. Pharmacophore models were constructed in MOE (13) using the consensus pharmacophore module. The Glide (14–16) docking algorithm at the XP level (17) was used to perform all docking calculations with UPPS. X-ray structures were prepared with the protein preparation wizard (18) using standard parameters. Compounds were prepared with LigPrep (19) using standard parameters. For the calculation of the ROC/AUC curves, 112 *E. coli* UPPS inhibitors with IC_{50} < 100 μM were combined with the Schrödinger decoy library of 1,000 compounds (having an average molecular mass of 400 Da) (14, 16). Compounds from this combined library were ranked by their Glide XP docking scores, and the AUC calculated.

Principal component analysis was performed using the monomer that had the most ligands present or, if not applicable, the most residues resolved. An invariant "core" of Cα atoms (20) was first determined, then structures were aligned with the core, and PCA analysis was performed using BIO3D (21). The principal components plotted in Fig. 8*B* describe orthogonal eigenvectors with maximal variance. Hierarchical clustering was performed based on the Euclidian distance matrix of the first two principal components, then reduced to three groups of related "clusters" (22).

Cell growth inhibition. The growth of *S. aureus* (USA300 strain) and determination of minimal inhibitory concentration (MIC) values were as described previously (23). *E. coli* growth and construction of isobolograms were also carried out basically as described previously (24).

In vivo experiments. Mice were infected i.p. with 10^9 cfu methicillin-resistant *Staphylococcus aureus* (strain Sanger 252) suspended in 4% hog gastric mucin. At 1 h after infection, the mice were divided into two groups (n = 10 per group) and treated i.p. with either **17** (10 mg/kg) suspended in water or water alone (vehicle control). Treatment was continued once daily for two more days. Mortality was monitored twice daily.

1. Durrant JD, et al. (2011) Non-bisphosphonate inhibitors of isoprenoid biosynthesis identified via computer-aided drug design. *Chem Biol Drug Des* 78(3):323–332.
2. Zhang Y, et al. (2012) HIV-1 integrase inhibitor-inspired antibacterials targeting isoprenoid biosynthesis. *ACS Med Chem Lett* 3(5):402–406.
3. Yang L, et al. (2008) Mechanism of a prototypical synthetic membrane-active antimicrobial: Efficient hole-punching via interaction with negative intrinsic curvature lipids. *Proc Natl Acad Sci USA* 105(52):20595–20600.
4. Pan JJ, Chiou ST, Liang PH (2000) Product distribution and pre-steady-state kinetic analysis of *Escherichia coli* undecaprenyl pyrophosphate synthase reaction. *Biochemistry* 39(35):10936–10942.
5. Otwinowski Z, Minor W (1997) Processing of X-ray diffraction data collected in oscillation mode. *Method Enzymol* 276(Macromol Crystallogr A):307–326.
6. Murshudov GN, Vagin AA, Dodson EJ (1997) Refinement of macromolecular structures by the maximum-likelihood method. *Acta Crystallogr D Biol Crystallogr* 53(Pt 3):240–255.
7. Potterton E, Briggs P, Turkenburg M, Dodson E (2003) A graphical user interface to the CCP4 program suite. *Acta Crystallogr D Biol Crystallogr* 59(Pt 7):1131–1137.
8. Adams PD, et al. (2010) PHENIX: A comprehensive Python-based system for macromolecular structure solution. *Acta Crystallogr D Biol Crystallogr* 66(Pt 2): 213–221.
9. Emsley P, Cowtan K (2004) COOT: Model-building tools for molecular graphics. *Acta Crystallogr D Biol Crystallogr* 60(Pt 12 Pt 1):2126–2132.
10. Delano WL (2008) *The PyMOL Molecular Graphics Systems* (DeLano Scientific LLC, Palo Alto, CA).
11. Webb MR (1992) A continuous spectrophotometric assay for inorganic phosphate and for measuring phosphate release kinetics in biological systems. *Proc Natl Acad Sci USA* 89(11):4884–4887.
12. Li H, et al. (2003) The effect of triton concentration on the activity of undecaprenyl pyrophosphate synthase inhibitors. *J Biomol Screen* 8(6):712–715.
13. Chemical Computing Group, Inc. (2006) *Molecular Operating Environment (MOE)* (Chemical Computing Group, Inc., Montreal).
14. Friesner RA, et al. (2004) Glide: A new approach for rapid, accurate docking and scoring. 1. Method and assessment of docking accuracy. *J Med Chem* 47(7):1739–1749.
15. Schrödinger LLC (2011) *Suite 2011: Glide, version 5.7* (Schrödinger LLC, New York).

16. Halgren TA, et al. (2004) Glide: A new approach for rapid, accurate docking and scoring. 2. Enrichment factors in database screening. *J Med Chem* 47(7):1750–1759.
17. Friesner RA, et al. (2006) Extra precision glide: Docking and scoring incorporating a model of hydrophobic enclosure for protein-ligand complexes. *J Med Chem* 49(21): 6177–6196.
18. Schrödinger, LLC (2011) Schrödinger Suite 2011 (Schrödinger, LLC, New York).
19. Schrödinger LLC (2011) *LigPrep, version 2.5* (Schrödinger LLC, New York).
20. Gerstein M, Altman RB (1995) Average core structures and variability measures for protein families: Application to the immunoglobulins. *J Mol Biol* 251(1):161–175.
21. Grant BJ, Rodrigues APC, ElSawy KM, McCammon JA, Caves LSD (2006) Bio3d: An R package for the comparative analysis of protein structures. *Bioinformatics* 22(21):2695–2696.
22. Murtagh F (1985) *Multidimensional Clustering Algorithms* (Physica, Würzburg, Germany).
23. Molohon KJ, et al. (2011) Structure determination and interception of biosynthetic intermediates for the plantazolicin class of highly discriminating antibiotics. *ACS Chem Biol* 6(12):1307–1313.
24. Leon A, et al. (2006) Isoprenoid biosynthesis as a drug target: Bisphosphonate inhibition of *Escherichia coli* K12 growth and synergistic effects of fosmidomycin. *J Med Chem* 49(25):7331–7341.

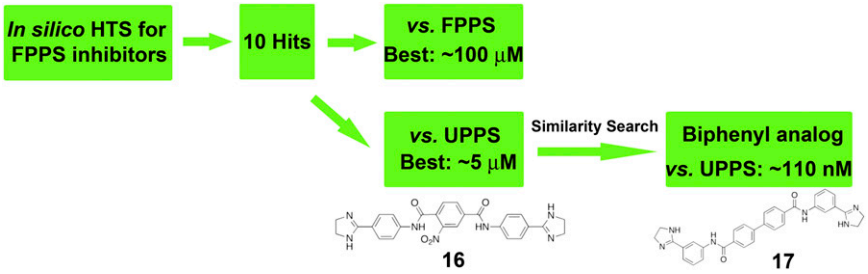

Fig. S1. Schematic illustration of hit-to-lead development. FPPS inhibitors obtained by *in silico* screening of the National Cancer Institute Diversity Set II were screened against *E. coli* UPPS basically as described previously (1): the most potent hit (~5 μM) was then used as a reference for a similarity search using SciFinder. A total of 22 compounds suggested were obtained from the National Institutes for Health Developmental Therapeutics Program. The most active lead was found to have ~110 nM IC_{50} values against both *E. coli* UPPS and *S. aureus* UPPS.

1. Durrant JD, et al. (2011) Non-bisphosphonate inhibitors of isoprenoid biosynthesis identified via computer-aided drug design. *Chem Biol Drug Des* 78(3):323–332.

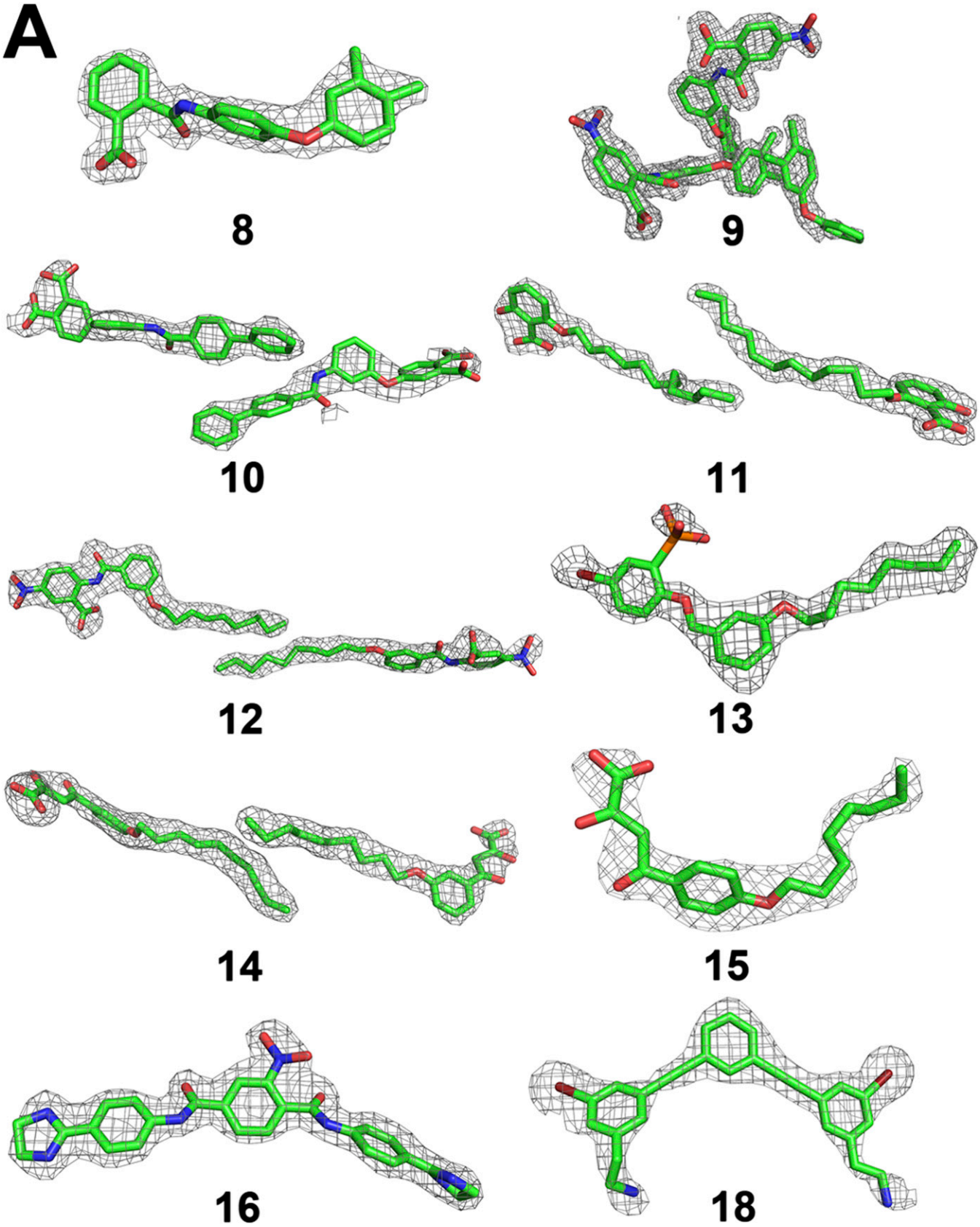

Fig. S2. (Continued)

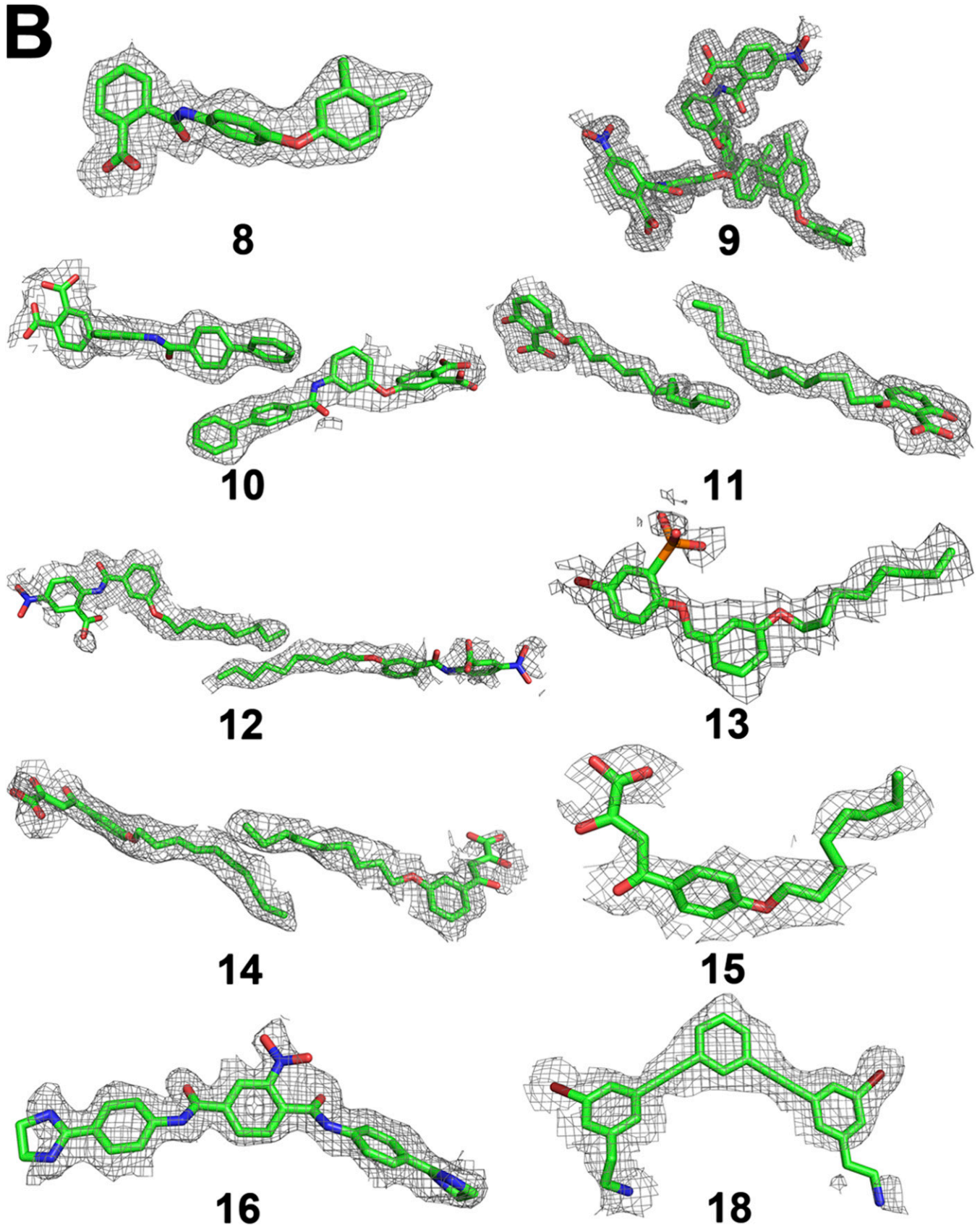

Fig. S2. (Continued)

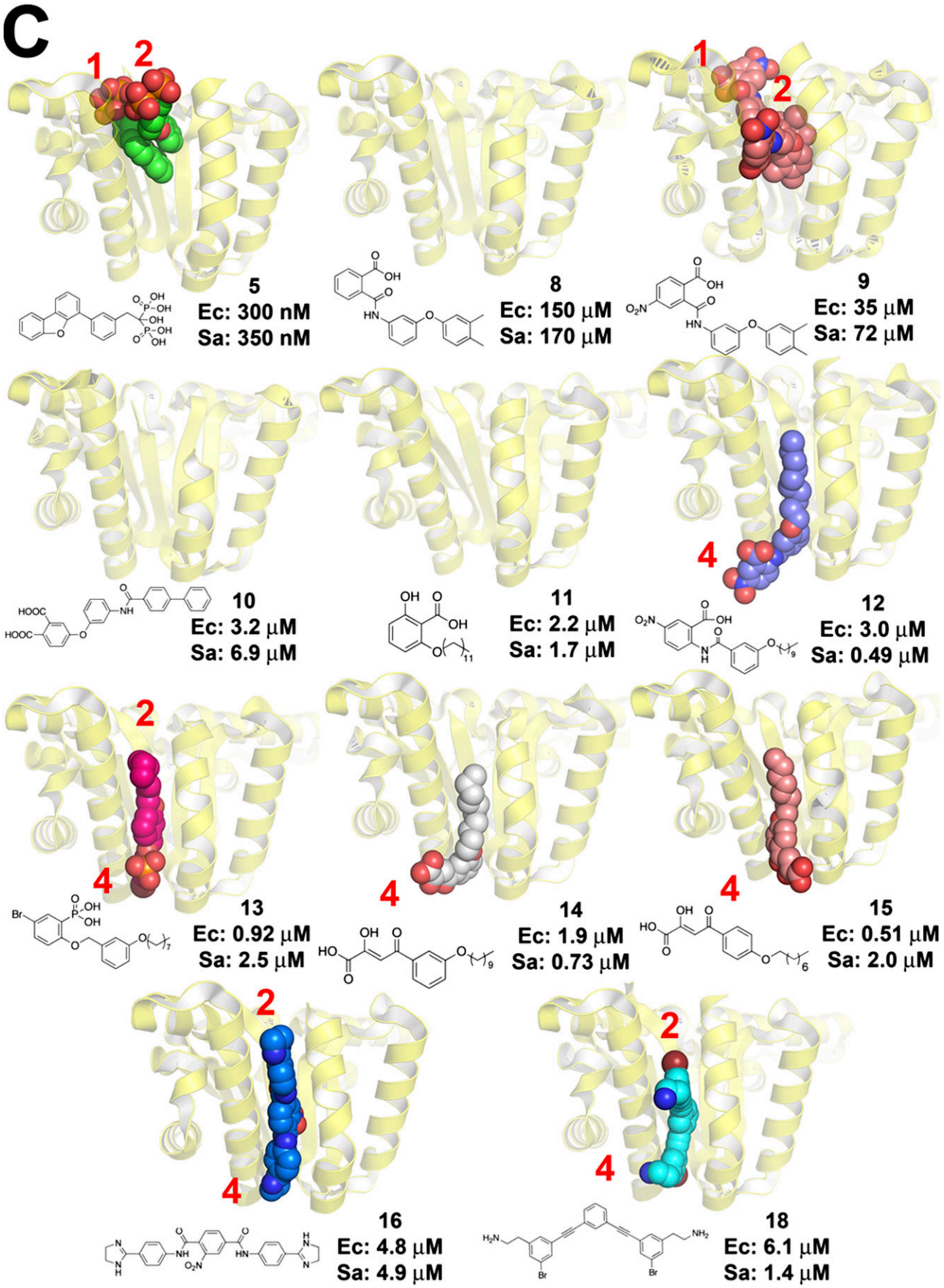

Fig. S2. (Continued)

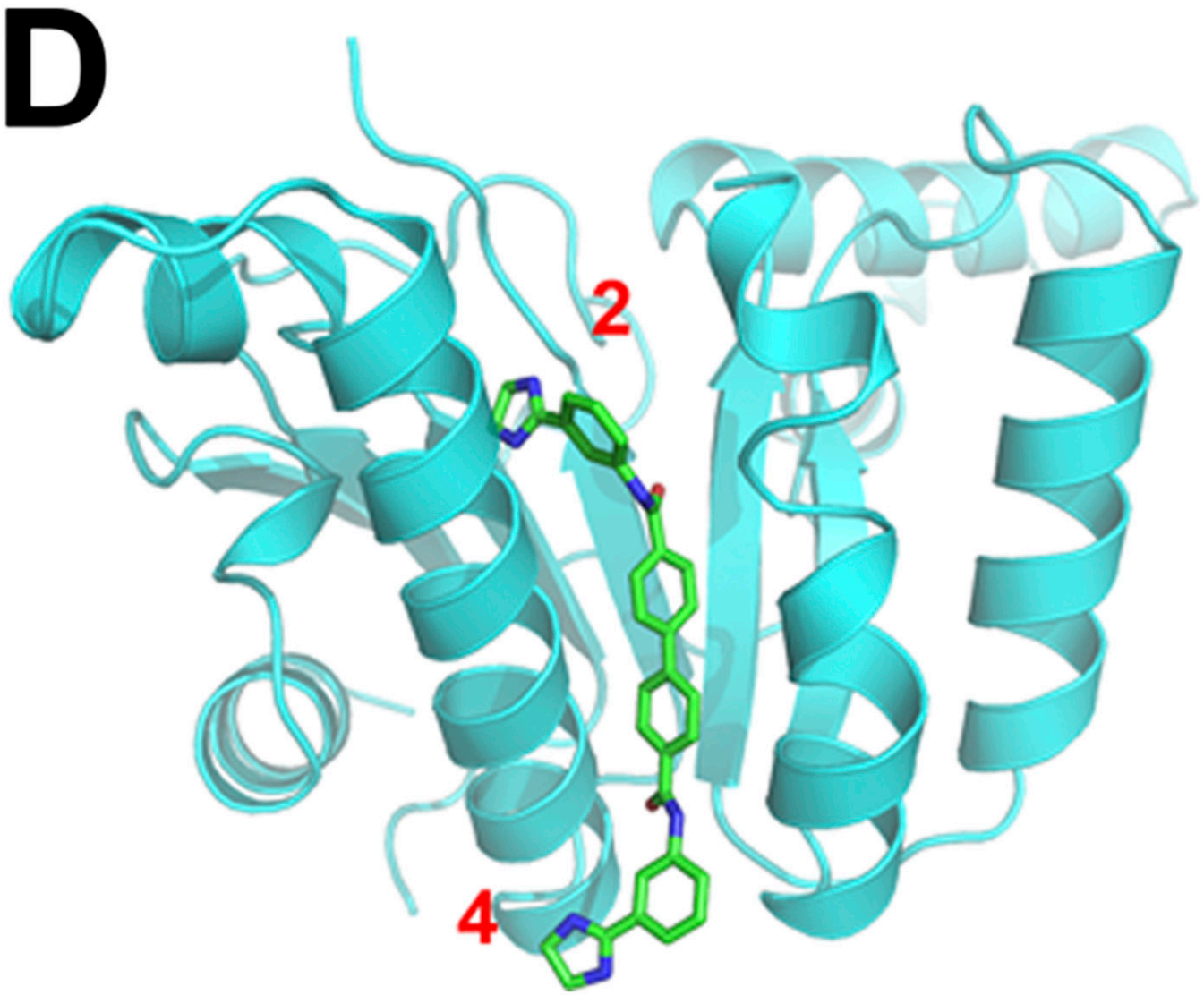

Fig. S2. (*A*) Electron density maps (2Fo-Fc) for compounds investigated contoured at 1σ. (*B*) Electron density maps (simulated-annealing Fo-Fc omit map) for compounds investigated contoured at 1σ. (*C*) Structures of inhibitors bound to *E. coli* UPPS. These sites typically are less highly occupied than those shown in the text. (*D*) Glide XP docking result for **17** bound to *E. coli* UPPS showing binding to sites 2 and 4.

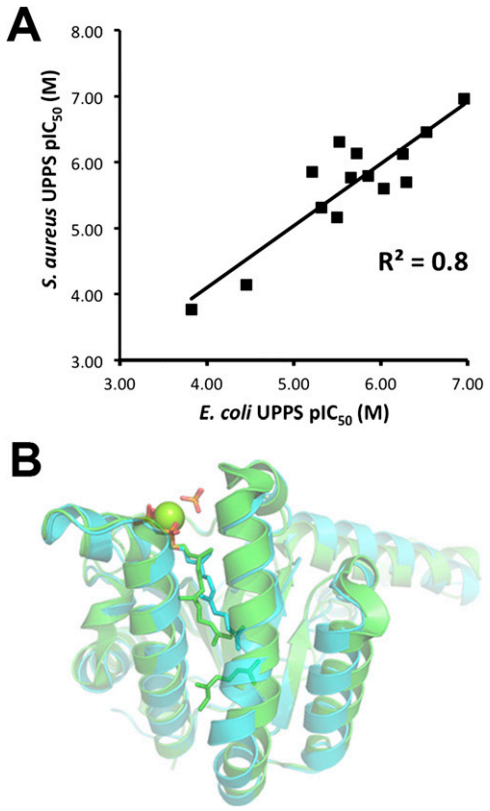

Fig. S3. (*A*) Correlation between *E. coli* and *S. aureus* UPPS inhibition by the compounds listed in Table S1. (*B*) Superimposition of *E. coli* UPPS structure (green, PDB ID code 1X06) and *S. aureus* UPPS structure (cyan, PDB ID code 4H8E). The Cα rmsd is 0.91 Å over 202 residues.

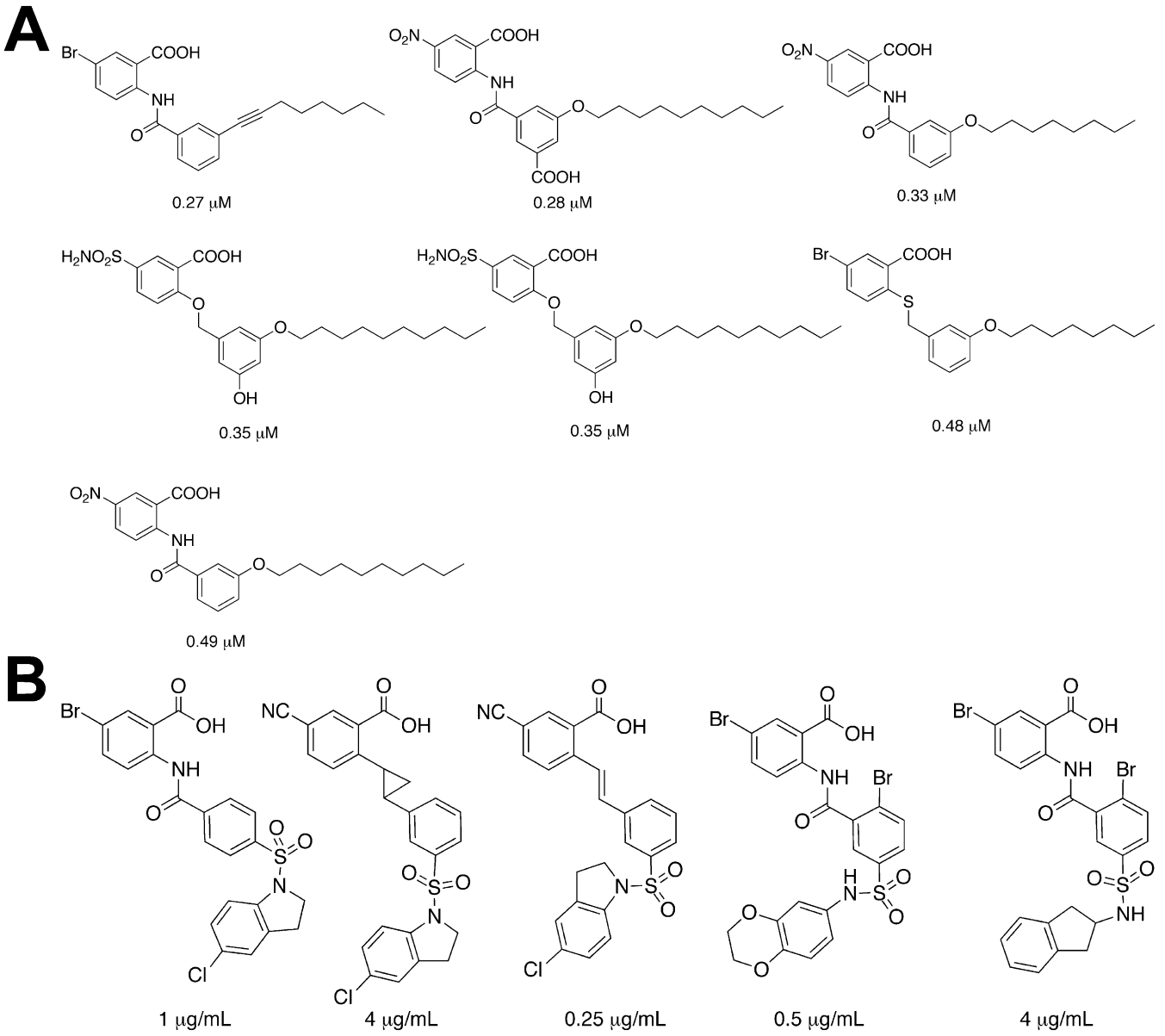

Fig. S4. (*A*) Structures of UPPS inhibitors used in pharmacophore modeling together with IC_{50} values (in *S. aureus* UPPS inhibition). (*B*) Structures of Larsen et al. (1) *S. aureus* benzoic acid growth inhibitors used to construct the pharmacophore model in Fig. 6*A*, together with MIC values (in cell growth inhibition).

1. Larsen SD, et al. (2006) Discovery and initial development of a novel class of antibacterials: Inhibitors of *Staphylococcus aureus* transcription/translation. *Bioorg Med Chem Lett* 16(24): 6173–6177.

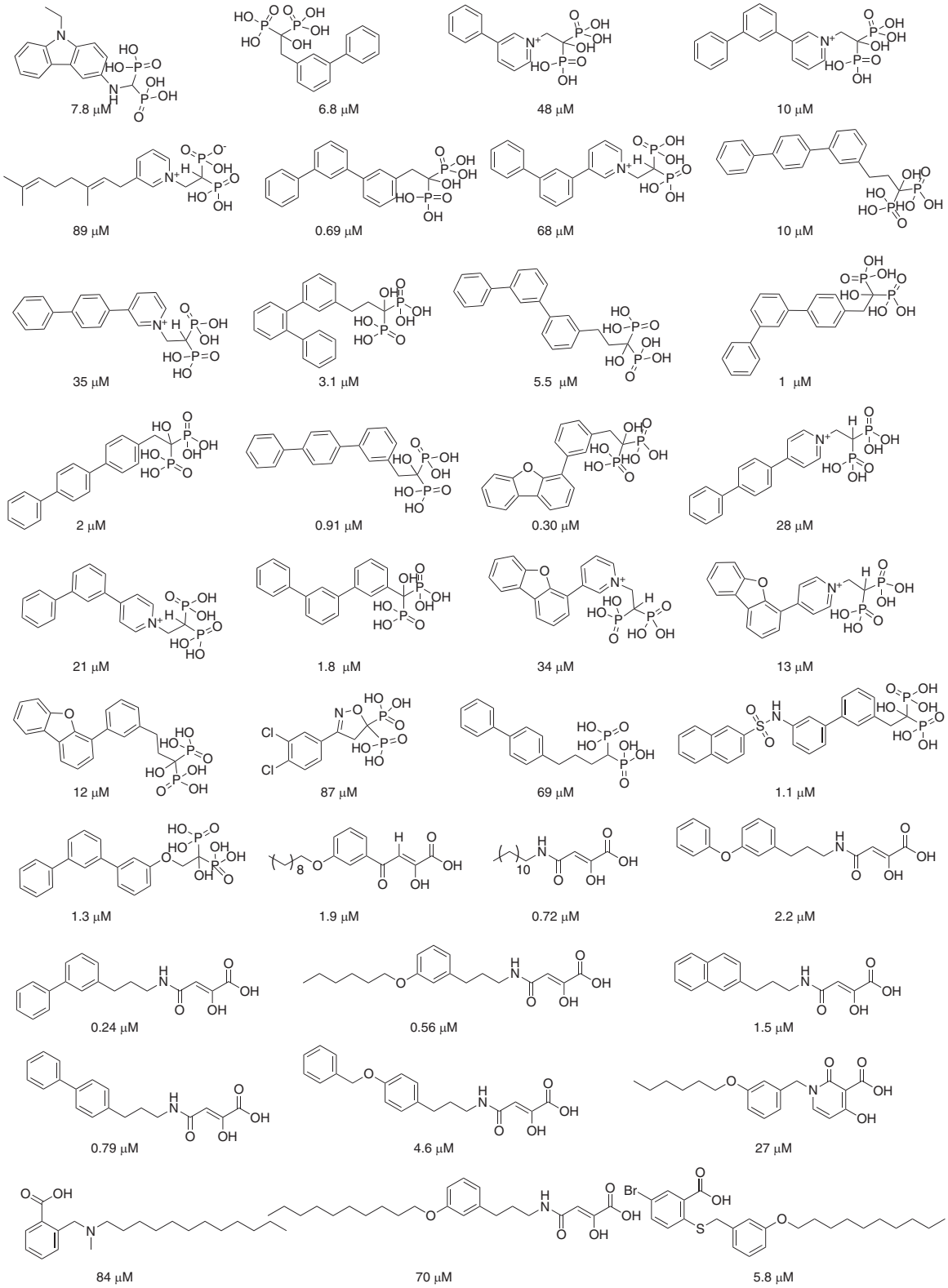

Fig. S5. (Continued)

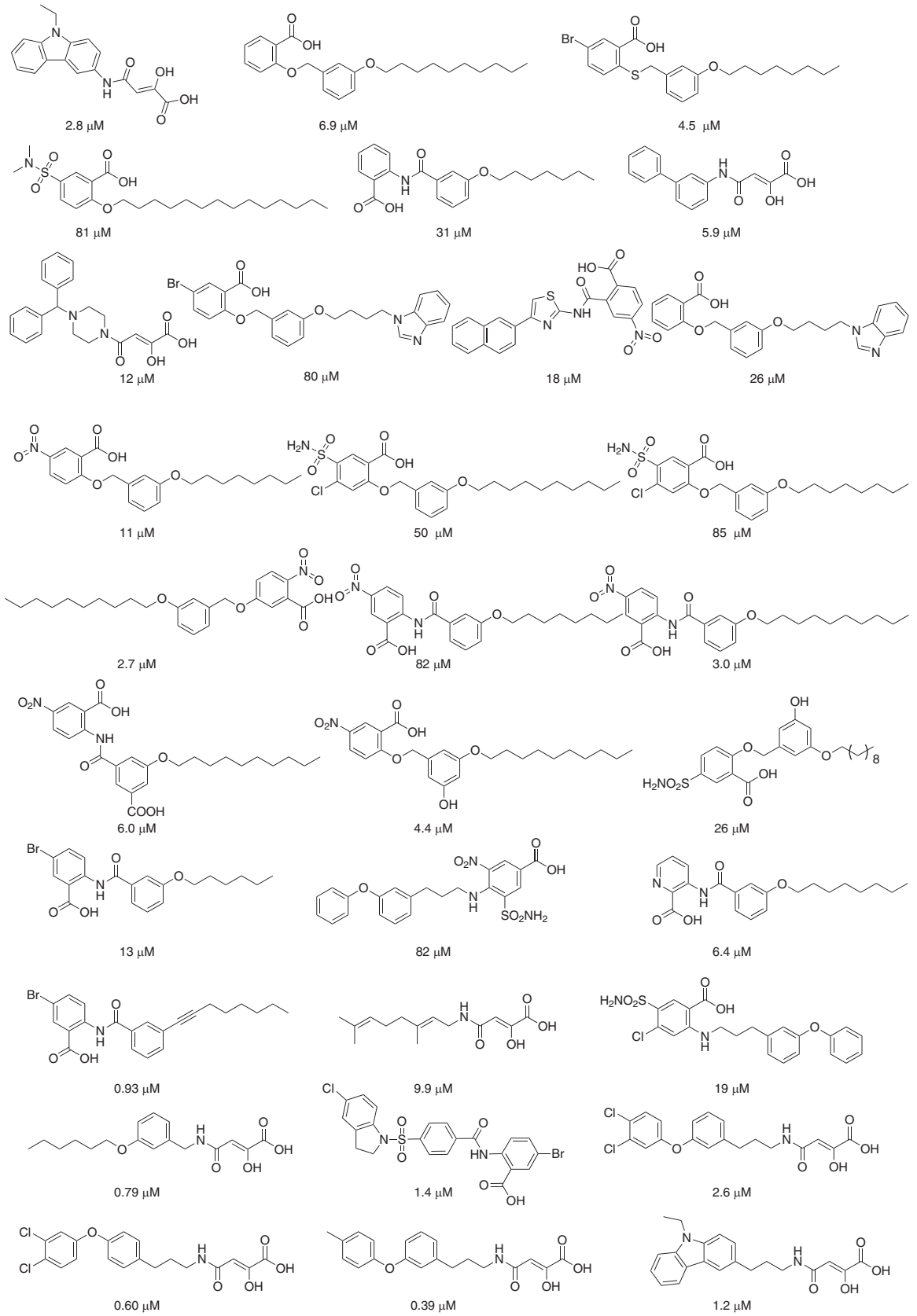

Fig. S5. (Continued)

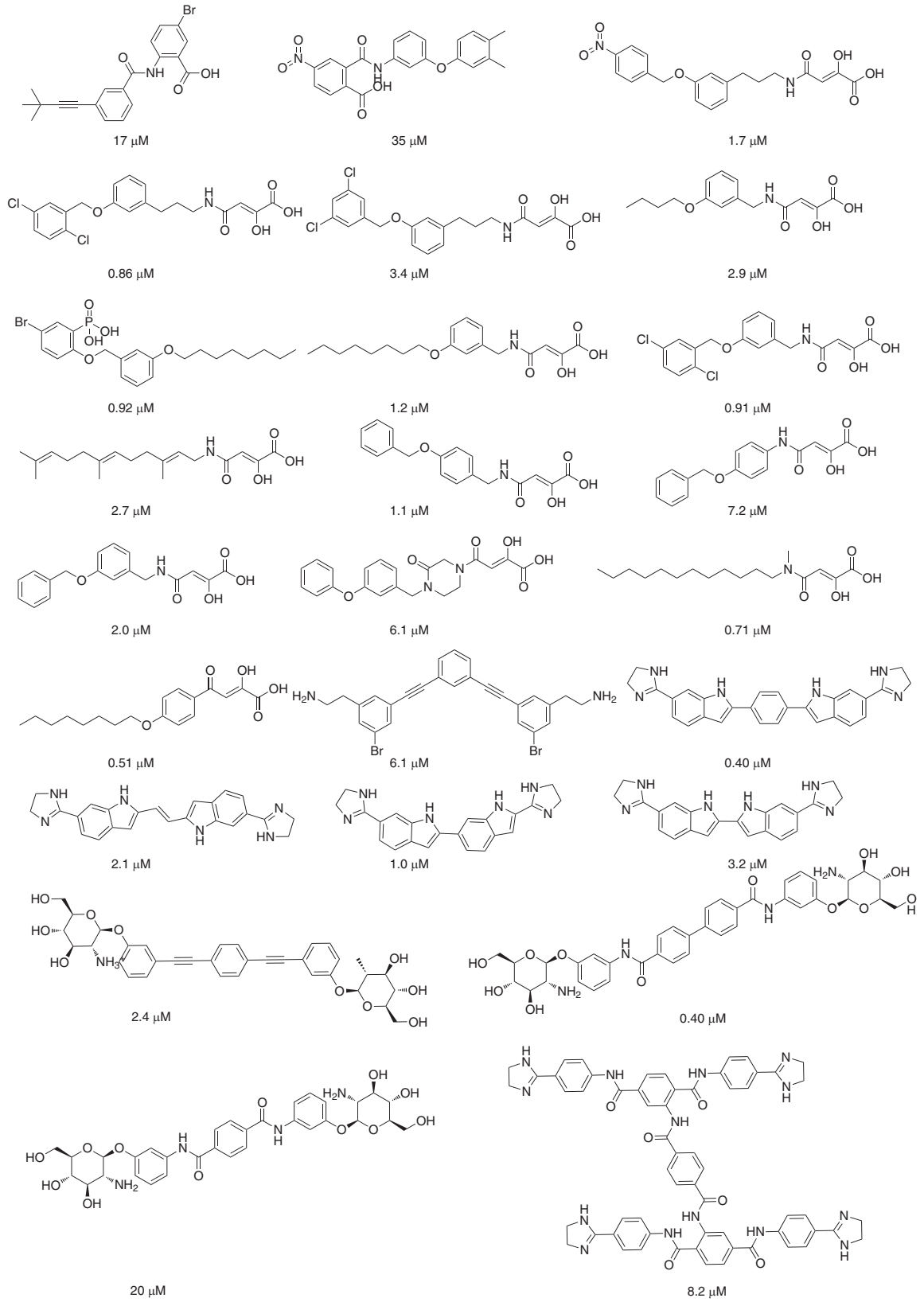

Fig. S5. (Continued)

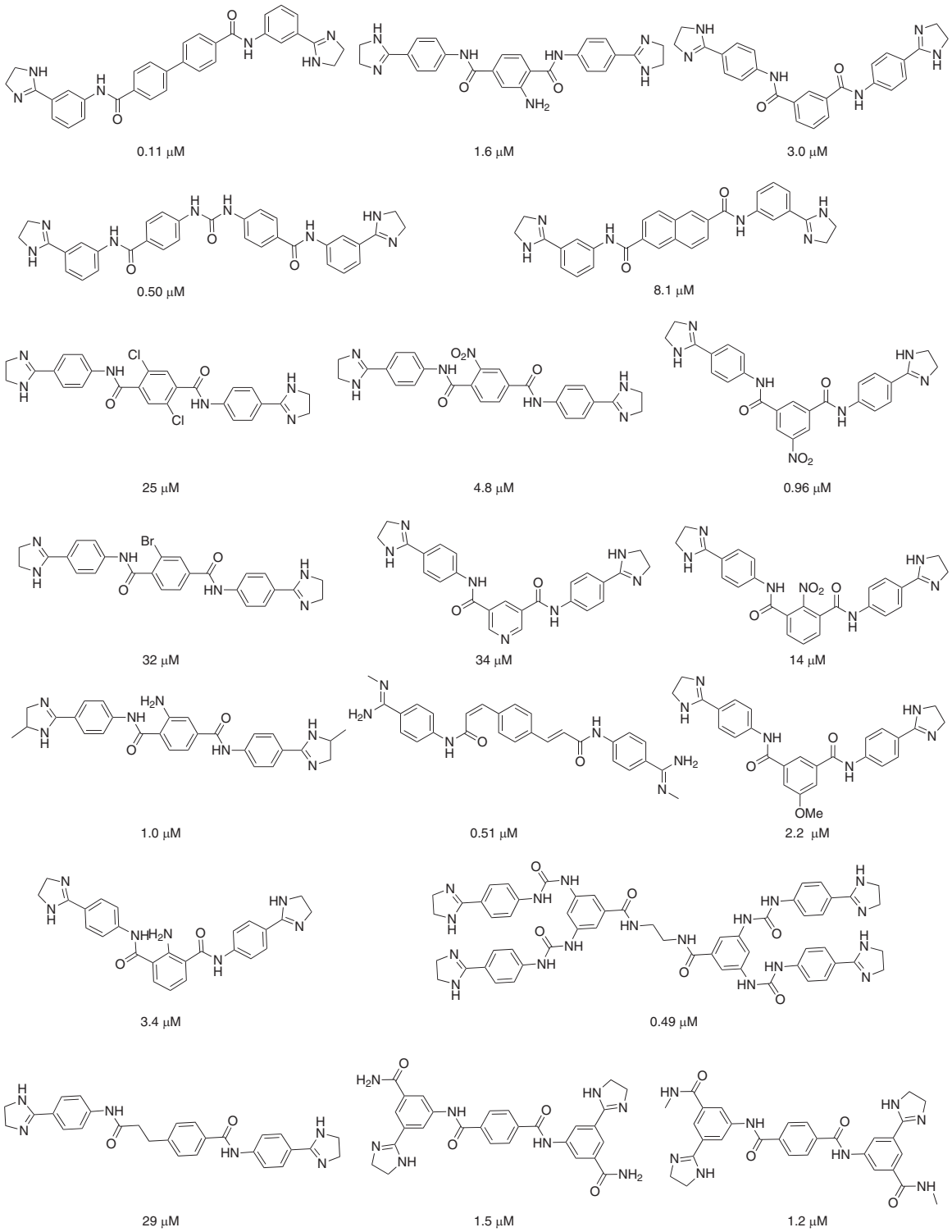

Fig. S5. Screening library used in ROC/AUC analysis. The IC_{50} values are for *E. coli* UPPS inhibition.

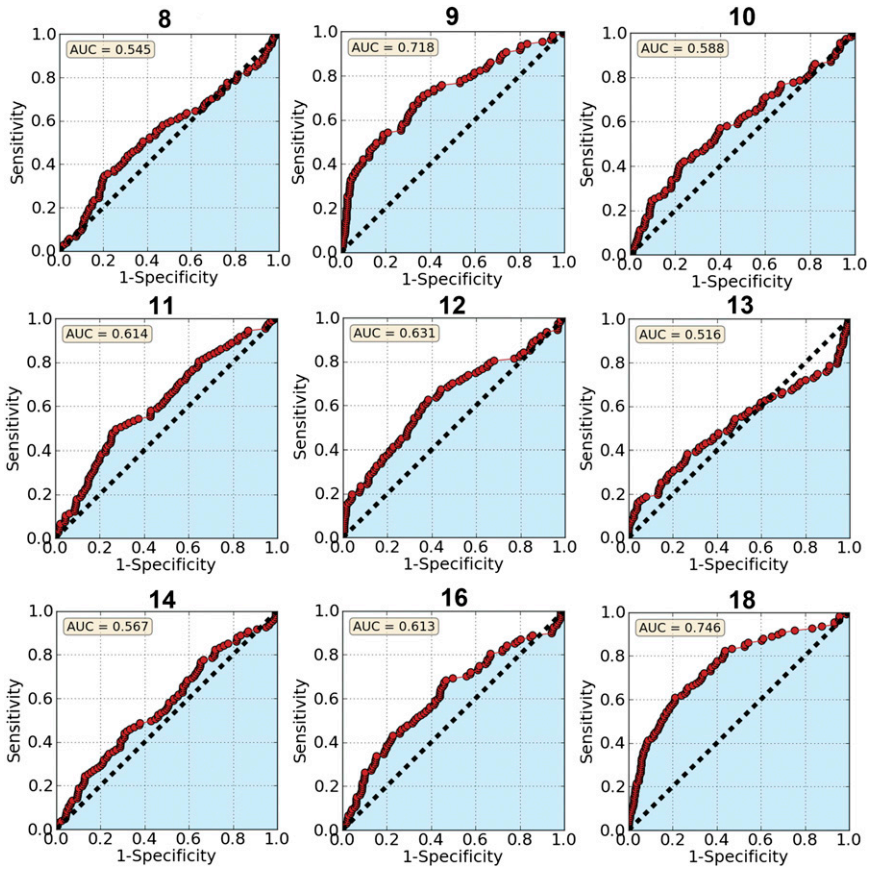

Fig. S6. ROC/AUC analyses for compounds shown in Fig. S6 based on the crystal structures reported in this work.

Table S1. Enzyme and cell growth inhibition results

	E. coli UPPS	*S. aureus* UPPS	*E. coli*	*S. aureus*
ID	IC_{50}, μM	IC_{50}, μM	MIC_{90}, μg/mL	MIC_{90}, μg/mL
5	0.30	0.35	>32	>32
7	0.56	0.75	>32	>32
8	150	170	>32	N.D.
9	35	72	>32	N.D.
10	3.2	6.9	16	N.D.
11	2.2	1.7	>32	N.D.
12	3.0	0.49	>32	>32
13	0.92	2.5	>32	32
14	1.9	0.73	>32	0.50
15	0.51	2.0	>32	0.25
16	4.8	4.9	8.0	>32
17	0.11	0.11	4.0	0.25
18	6.1	1.4	8.0	>32
19	1.4	1.6	>32	1.0

N.D., not determined.

Table S2. Data collection and refinement statistics for *E. coli* UPPS

Crystals	EcUPPS/**8** (3SGT)	EcUPPS/**9** (3SGV)	EcUPPS/**10** (3SGX)	EcUPPS/**11** (3SH0)	EcUPPS/**12** (4H2O)
Data collection					
Space group	$P2_12_12_1$	$P2_12_12_1$	$P2_12_12_1$	$P2_12_12_1$	$P2_12_12_1$
Unit cell dimension					
a, *b*, *c*, Å	62.92, 68.35, 111.98	63.14, 69.00, 112.56	60.95, 68.14, 111.61	62.77, 68.72, 112.06	63.38, 68.37, 109.94
X-ray source	APS 21-ID-G	APS 21-ID-F	APS 21-ID-F	APS 21-ID-D	APS 21-ID-F
Wavelength, Å	0.97857	0.97857	0.97857	0.97857	0.97857
Resolution (Å)*	50.0–1.85 (1.88–1.85)	50.0–1.61 (1.64–1.61)	50.0–2.45 (2.49–2.45)	50.0–1.84 (1.87–1.84)	50.0–2.14 (2.18–2.14)
No. of reflection observed	348, 506	956, 565	98,722	423, 643	371,965
Unique	41,827 (1,909)	62,778 (2,554)	17,225 (786)	42,560 (1,870)	26,986 (1319)
Completeness (%)	99.5 (93.4)	97.6 (80.5)	96.9 (90.7)	99.3 (89.2)	99.7 (99.4)
R-merge	0.067 (0.502)	0.095 (0.704)	0.092 (0.451)	0.065 (0.642)	0.082 (0.594)
I/σ(I)	41.7 (2.5)	35.4 (1.4)	23.3 (2.8)	28.9 (1.4)	30.7 (5.3)
Multiplicity	8.3 (5.1)	15.2 (5.6)	5.7 (4.7)	10.0 (5.3)	13.8 (13.5)
Refinement statistics					
Resolution range, Å	35.68–1.85	43.61–1.61	32.65–2.45	35.71–1.84	46.48–2.14
R_{work}/R_{free}, %	17.4/22.7	17.4/21.4	24.2/32.8	16.8/21.1	23.2/29.5
Rmsd					
Bond lengths	0.024	0.026	0.015	0.024	0.017
Bond angles	1.851	2.249	1.682	1.901	1.92
No. of atoms					
Protein	3,413	3,487	3,256	3,397	3,217
Ligand	27	135	68	69	96
Occupancy of ligand	1.0	1.0	1.0	1.0	1.0
B average, Å^2: protein	32.30	25.21	46.07	30.54	38.76
B average, Å^2: ligand	37.25	33.60	59.17	41.17	74.15
Crystals	EcUPPS/**13** (4H38)	EcUPPS/**14** (4H3C)	EcUPPS/**15** (4H3A)	EcUPPS/**16** (4H2J)	EcUPPS/**18** (4H2M)
Data collection					
Space group	$P2_12_12_1$	$P2_12_12_1$	$P2_12_12_1$	$P2_12_12_1$	$P2_12_12_1$
Unit cell dimension					
a, *b*, *c*, Å	63.26, 68.82, 111.49	63.33, 69.10, 111.69	62.98, 68.71, 111.92	68.16, 68.96, 111.74	62.83, 68.89, 112.02
X-ray source	APS 21-ID-F	APS 21-ID-G	APS 21-ID-G	APS 21-ID-F	APS 21-ID-G
Wavelength, Å	0.97857	0.97857	0.97857	0.97857	0.97857
Resolution (Å)	50.0–1.95 (1.98–1.95)	50.0–1.93 (1.96–1.93)	50.0–1.98 (2.01–1.98)	50.0–1.81 (1.84–1.81)	50.0–1.78 (1.81–1.78)
No. of reflections observed	262,481	542,651	493,329	396,626	375,414
Unique	36,240 (1,786)	37,169 (1,846)	34,503 (1,700)	45,055 (2,204)	47,258 (2,312)
Completeness (%)	99.8 (100.0)	99.3 (99.1)	100.0 (100.0)	99.6 (100.0)	99.9 (98.8)
R_{merge}	0.091 (0.642)	0.083 (0.637)	0.059 (0.635)	0.076 (0.698)	0.066 (0.670)
I/σ(I)	20.4 (4.1)	34.2 (6.6)	39.7 (4.3)	27.8 (4.7)	29.1 (2.6)
Multiplicity	7.2 (7.4)	14.6 (14.4)	14.3 (14.2)	8.8 (9.0)	7.9 (6.3)
Refinement statistics					
Resolution range, Å	34.41–1.95	43.43–1.93	46.43–1.98	30.39–1.81	43.46–1.78
R_{work}/R_{free}, %	20.6/26.2	20.6/25.0	20.9/24.9	19.7/23.4	20.4/24.2
Rmsd					
Bond lengths	0.020	0.022	0.019	0.023	0.024
Bond angles	1.953	2.092	1.855	2.262	2.116
No. of atoms					
Protein	3,324	3,257	3,211	3,360	3,353
Ligand	28	75	46	74	60
Occupancy of ligand	1.0	1.0	1.0	1.0	1.0
B average, Å^2: protein	28.91	33.39	39.08	28.08	29.14
B average, Å^2: ligand	68.04	58.51	69.71	53.85	63.86

*Values in the parentheses are for the highest-resolution shells.

Table S3. SCORECONS using *E. coli* UPPS as a target

Ranking	Residue no.	SCORECONS score (1)	Residue	Alignment
1	26	0.988	D	DDDDDDDDDDDDDDDDDDDDDDDDDDDDDDDDDD
2	30	0.984	R	RRRRRRRRRRRRRRRRRRRRRRRRRRRRRRRRRR
3	28	0.976	N	NNNNNNNNNNNNNNNNNNNNNNNNNNNNNNNNNN
4	74	0.968	N	NNNNNNNNNNNNNNNNNNNNNNNNNNNNNNNNNN
5	20	0.964	H	HHHHHHHHHHHHHHHHHHHHHHHHHHHHHHHHHH
6*	190	0.960	D	DDDDDDDEDDDDEDDDDEDDDDDDDDEDDDDDDD
7	77	0.953	R	RRRRRRRRRRRRRRRRRRRRRRRRRRRRRRRRRR
8	204	0.945	F	FFFFFFFFFFFFFFFFFFFYFFFFFFFFFFFFFFFFFFFFFY
9	145	0.941	Y	YYYYYYYYYYYYYYYYYYYYYYYYYYYYYYYYYYYYYYYYY
10	194	0.937	R	RRRRRRRRRRRRRRRRRRRRRRRRRRRRRRRRRR
11	200	0.933	R	RRRRRRRRRRRRRRRRRRRRRRRRRRRRRRRRRR
12	202	0.925	S	SSSSSSSSSSSSSSSSSSSSSSSSSSSSSSSSSSSSSSSSSS
13*	18	0.921	C	CPPPPPPPPPPPPPPPPPPPPPPPPPPPPPPPPPP
14	71	0.917	S	SSSSSSSSSSSSSSSSSSSSSSSSSSSSSSSSSSSSSSSSSS
15	32	0.905	A	AAAAAAAAAAAAAAAAAAAAAAAAAAAAGAAAAAA
16	207	0.901	W	WWWWWWWWWWWWWWWWWWWWWWWWWW
17	221	0.897	W	WWWWWWWWWWWWWWWWWWWWWWWWWW
18	81	0.889	E	EEEEEEEEEEEEEEEEEEEEEEEEEEEEEEEEEE
19	43	0.881	H	HHHHHHHHHHHHHHHHHHHHHHHHHHHHHHHHHH
20	66	0.874	T	TTTTTTTTTTTTTTTTTTTTTTTTTTTTTTTTTSTTTTTTT

Asp26 is the most essential residue and binds to Mg^{2+} in the active site.
*Residues are different in *E. coli* UPPS and *S. aureus* UPPS.

1. Valdar WSJ (2002) Scoring residue conservation. *Proteins* 48(2):227–241.

Table S4. Data collection and refinement statistics for *S. aureus* UPPS

Crystals	SaUPPS/FPP (4H8E)
Data collection	
Space group	$P4_12_12$
Unit cell dimension	
a, *b*, *c*, Å	57.303, 57.303, 158.824
X-ray source	APS 21-ID-G
Wavelength, Å	0.97857
Resolution (Å)*	50.00–1.30 (1.32–1.30)
No. of reflection observed	916,358
Unique	66,126 (3,237)
Completeness (%)	100.0 (100.0)
R_{merge}	0.077 (0.400)
I/σ(I)	33.9 (5.3)
Multiplicity	13.9 (11.3)
Refinement statistics	
Resolution range, Å	32.64–1.30
R_{work}/R_{free}, %	17.4/19.4
Rmsd	
Bond lengths	0.032
Bond angles	2.655
No. of atoms	
Protein	1,918
Ligand	30
Occupancy of ligand	1.0
B average, Å^2: protein	13.11
B average, Å^2: ligand	11.70

*Values in parentheses are for the highest-resolution shells.